

A rice single cell transcriptomic atlas defines the developmental trajectories of rice floret and inflorescence meristems

Jie Zong^{1*} , Li Wang^{1*} , Lu Zhu^{1*} , Lianle Bian², Bo Zhang², Xiaofei Chen¹ , Guoqiang Huang¹ , Xuelian Zhang¹ , Junyi Fan¹ , Liming Cao³ , George Coupland⁴ , Wanqi Liang¹ , Dabing Zhang^{1,5} and Zheng Yuan¹

¹Joint International Research Laboratory of Metabolic & Developmental Sciences, State Key Laboratory of Hybrid Rice, School of Life Sciences and Biotechnology, Shanghai Jiao Tong University, Shanghai 200240, China; ²NovelBio Bio-Pharm Technology Co. Ltd, Shanghai 201114, China; ³Crop Breeding & Cultivation Research Institute, Shanghai Academy of Agriculture Sciences, Shanghai 201403, China; ⁴Max Planck Institute for Plant Breeding Research, Cologne D50829, Germany; ⁵School of Agriculture, Food and Wine, University of Adelaide, Waite Campus, Urrbrae, SA 5064, Australia

Summary

Author for correspondence:
 Zheng Yuan
 Email: zyuan@sjtu.edu.cn

Received: 18 October 2021
 Accepted: 19 January 2022

New Phytologist (2022) **234**: 494–512
 doi: 10.1111/nph.18008

Key words: axillary meristem, differentiation trajectory, rice inflorescence, scRNA-seq, spikelet.

- Rice inflorescence development determines yield and relies on the activity of axillary meristems (AMs); however, high-resolution analysis of its early development is lacking.
- Here, we have used high-throughput single-cell RNA sequencing to profile 37 571 rice inflorescence cells and constructed a genome-scale gene expression resource covering the inflorescence-to-floret transition during early reproductive development. The differentiation trajectories of florets and AMs were reconstructed, and discrete cell types and groups of regulators in the highly heterogeneous young inflorescence were identified and then validated by *in situ* hybridization and with fluorescent marker lines.
- Our data demonstrate that a WOX transcription factor, DWARF TILLER1, regulates flower meristem activity, and provide evidence for the role of auxin in rice inflorescence branching by exploring the expression and biological role of the auxin importer OsAUX1.
- Our comprehensive transcriptomic atlas of early rice inflorescence development, supported by genetic evidence, provides single-cell-level insights into AM differentiation and floret development.

Introduction

The architecture of the grass inflorescence depends on the activities of the indeterminate inflorescence meristem (IM; also called the rachis meristem), the auxiliary primary and secondary branch meristems, and the transition to the determinate spikelet meristem (Zhang & Yuan, 2014; B. Wang *et al.*, 2018; Yuan *et al.*, 2020; Zhu & Wagner, 2020). In rice (*Oryza sativa*), the IM initiates inflorescence development. All lateral organs are derived from axillary meristems (AMs) (Kyozuka *et al.*, 2014; B. Wang *et al.*, 2018; Zhu & Wagner, 2020); the only structure in the rice inflorescence not derived from an AM is the rachis, the central structure generated by the IM. The IM generates a series of AMs that produce branches, such as the primary branch meristem (PBM), the elongated primary branch meristem (ePBM), and the secondary branch meristem (SBM) from branch meristems (BMs); or spikelets and flowers, from the spikelet meristem (SM) and floret meristem (FM), respectively (Tanaka *et al.*, 2013; Kyozuka *et al.*, 2014) [Correction added after first publication 24 February 2022: a reference has been deleted from the preceding sentence.]. Spatiotemporal changes in several phytohormones, including cytokinin (CK), GA, brassinosteroids, and jasmonic

acids, are known to affect AM activity and transition time (Tanaka *et al.*, 2013; Kyozuka, 2014; Zhang & Yuan, 2014; Yuan *et al.*, 2020). Transcription factors (TFs), such as members of the SQUAMOSA PROMOTER BINDING PROTEIN-LIKE (SPL), basic helix-loop-helix, APETALA2/ETHYLENE RESPONSE FACTOR (AP2/ERF), TEOSINTE BRANCHED1/CYCLOIDEA/PROLIFERATING CELL FACTOR 1, and MADS-box families, integrate environmental and hormonal information to orchestrate AM identity, activity, and determinacy to regulate inflorescence and spikelet development (B. Wang *et al.*, 2018; Yuan *et al.*, 2020; Zhu & Wagner, 2020) [Correction added after first publication 24 February 2022: a reference has been deleted from the preceding sentence.].

Single-cell RNA sequencing (scRNA-seq) technology has recently been used to examine the cellular identity and heterogeneity of several complex plant tissues in maize (*Zea mays*) (Nelms & Walbot, 2019; Satterlee *et al.*, 2020; Marand *et al.*, 2021; Xu *et al.*, 2021), Arabidopsis (Denyer *et al.*, 2019; Zhang *et al.*, 2019, 2021b; Satterlee *et al.*, 2020), and rice (Liu *et al.*, 2021; Wang *et al.*, 2021; Zhang *et al.*, 2021a). These studies not only provide valuable transcriptomic information at single-cell resolution, but also provide unprecedented insights into the developmental trajectory of key plant organs (Seyfferth *et al.*, 2021; Shaw *et al.*, 2021). Here, we have used scRNA-seq to unravel the identities,

*These authors contributed equally to this work.

distribution, and development of rice inflorescence cells to reconstruct the differentiation trajectory of floret and meristem cells.

Materials and Methods

Plant materials and growth conditions

All rice (*O. sativa* L. ssp. *japonica*) varieties, including wild-type variety 9522, *Osaux1-1;1* and *Osaux1-1;3* mutant (Giri *et al.*, 2018), and *dwarf tiller1* (*dwt1*) mutant (Wang *et al.*, 2014) lines, were planted in the paddy fields of Shanghai Jiao Tong University (30°N, 121°E) during the normal growing season (June–September).

Mutant generation and analysis

Clustered regularly interspaced short palindromic repeat (CRISPR)-CRISPR-associated protein 9 (Cas9) genome editing, as described previously (Xie *et al.*, 2015), was used to obtain the *Osaux1-1;4* mutant in cv 9522. Stable *Agrobacterium*-mediated transformation was performed in rice as described previously (Hiei & Komari, 2008). Plants from both T₀ and T₁ generations were screened by PCR. More than 100 spikelets from 10 individual lines were observed for phenotyping analysis. A Leica S8 APO stereomicroscope (Leica, Wetzlar, Germany) was used to take photographs. Phenotypic analyses were performed at grain maturity, using 10 panicles from 10 individual plants. Statistical analyses of significance were performed using Student's *t*-test. Single guide RNA sequence and PCR primer sequence are listed in Supporting Information Table S1.

The enhanced green fluorescent protein (eGFP) reporters under control of both *OsMAPK6* and *OsGASR1* promoters were generated by cloning *OsMAPK6* and *OsGASR1* promoter sequence, respectively, into the binary vector *pCAMBIA1301:eGFP* using *HindIII* and *Spel* restriction sites with the In-Fusion HD Cloning Kit (Takara, Shiga, Japan). The resulting constructs were stably transformed into cv 9522 using *Agrobacterium*-mediated transformation as previously described (Hiei & Komari, 2008). eGFP signals were captured using an Olympus IXplore SpinSR microscope (Olympus, Tokyo, Japan) in <5 mm inflorescences (excitation 488 nm and emission 500–530 nm wavelengths). The primers used are listed in Table S1.

Single-cell dissociation

Two replicate inflorescence samples were staged by length to coincide with commencement of branching, spikelet, and floret meristem development (Ikeda *et al.*, 2004): stage 1 (S1), <2 mm; stage 2 (S2), 2–3 mm. As bracts could not be removed from the inflorescence (Ikeda *et al.*, 2004), a single young flag leaf (L) covering the inflorescence was used as the control. Each replication contains around 100 young inflorescences or leaves. For protoplast isolation, samples were first cut into small pieces with a fresh sharp razor blade and then digested at room temperature in RNase-free enzyme solution (1.5% (w/v) cellulase R-10, 1% (w/v) macerozyme R-10 (Yakult), 0.4 M mannitol, 20 mM MES pH 5.7, 20 mM potassium chloride, 10 mM calcium chloride,

0.1% BSA (Sigma-Aldrich)). Protoplasts were filtered using a 45 µm cell strainer (Biologix, Biologix Group Ltd, Jinan, China) and centrifuged at 200 g for 3 min. After the supernatant was removed, the pellet was washed three times with 8% (w/v) mannitol, and cell viability was determined by acridine orange–propidium iodide staining (Countstar® Rigel; ALIT Life Science, Shanghai, China). Digestion progress was assayed every hour for 6 h, with the optimum time for cell viability, and the chosen optimum protoplast digestion time was 2 h (Fig. S1a).

Single-cell RNA sequencing

The concentration of protoplasts for sequencing was adjusted to c. 1000 µl⁻¹ with >80% viability. The BD Rhapsody system (BD Life Sciences, San Jose, CA, USA) was used to capture transcriptomic information from the protoplasts using a simple cartridge workflow and a multitier barcoding system (Shum *et al.*, 2019). In general, single-cell capture was achieved by random distribution of a single-cell suspension across >200 000 microwells through a limited dilution approach. Beads with oligonucleotide barcodes were added to saturation so that a bead was paired with a cell in a microwell. Cells were lysed in the microwell to hybridize messenger RNA (mRNA) molecules to barcoded capture oligonucleotides on the beads. Beads were collected into a single tube for reverse transcription and *ExoI* digestion to clean extra polyT primers. During complementary DNA (cDNA) synthesis, each cDNA molecule was tagged at the 5' end (i.e. the 3' end of a mRNA transcript) with a unique molecular identifier (UMI) and barcode indicating its cell origin. Libraries were prepared using the BD Rhapsody single-cell whole-transcriptome amplification (WTA) workflow, including random priming and extension (RPE), RPE amplification PCR, and WTA index PCR. Libraries were quantified using a High Sensitivity DNA chip (Agilent Technologies Inc., Palo Alto, CA, USA) on a Bioanalyzer 2200 and the Qubit High Sensitivity DNA assay (Thermo Fisher Scientific, Waltham, MA, USA). Sequencing was performed using an Illumina sequencer on a 150 bp paired-end run.

Single-cell RNA expression analysis

The software FASTP with default parameters (Chen *et al.*, 2018) was applied to filter the adapter sequences and remove low-quality reads to achieve the clean data, and UMI_TOOLS (Smith *et al.*, 2017) was used for single-cell transcriptome analysis to identify the cell barcode whitelist. The UMI-based clean data were mapped to the IRGSP1.0 genome (<https://rapdb.dna.affrc.go.jp/download/irgsp1.html>; Sakai *et al.*, 2013) using STAR with default parameters (Dobin *et al.*, 2013) from the UMI_TOOLS standard pipeline to obtain the UMI counts of each sample. Cell quality thresholds were set at >200 expressed genes and <20% mitochondrial UMI rate (mito %); mitochondrial genes were removed in the expression table. The SEURAT package (v.2.3.4, <https://satijalab.org/seurat/>; Satija *et al.*, 2015) was used for cell normalization and regression based on the UMI counts for each sample and mito % to obtain the scaled data, which was normalized by the function NormalizeData for further analysis. The

function FindVariableGenes was used to calculate highly variable genes (HVGs) across the single cells (<https://scrnaseq-course.cog.sanger.ac.uk/website/seurat-chapter.html>).

Principal component analysis (PCA) for all cells were constructed based on the scaled data with the top 1000 HVGs, and the top 10 principal components were used for *t*-distributed stochastic neighbour embedding construction and uniform manifold approximation and projection (UMAP) construction (van der Maaten & Hinton, 2008; Becht *et al.*, 2018). Unsupervised cell cluster results were generated based on the PCA top 10 principal components by applying the graph-based cluster method (resolution 0.8) in the SEURAT package. Marker genes were identified with the SEURAT FindAllMarkers function using the Wilcox rank sum test algorithm with the following parameters: ‘log_e(fold change)’ > 0.25; ‘min.pct’ > 10%; and ‘P-value’ < 0.01. Inflorescence clusters of the same cell type were selected for reanalysis with PCA, graph-based clustering, and marker identification to further refine cell identity. METANEIGHBOR analysis (Crow *et al.*, 2018) was performed with R script from <https://github.com/maggiecrow/MetaNeighbor/>, using variable genes selected through SEURAT to test cell-type clusters identity between replications of samples S1 and S2.

Protoplast preparation has been shown to trigger protoplasting-responsive genes not present during normal plant growth (Xu *et al.*, 2021). To avoid interference of these genes on subsequent analyses, protoplasting-responsive genes from maize datasets (Xu *et al.*, 2021) were used to identify rice homologues from the rice proteomes database (<https://rapdb.dna.affrc.go.jp>) using BLASTP with the following parameters: criteria *E*-value < 1E-50; identity > 70%; query cover > 70%; subject cover > 70%. This analysis resulted in a list of 332 genes (Table S2), which were excluded for further analyses.

Differential expression analysis

Differentially expressed genes (DEGs) were identified with the SEURAT FindMarkers function using the Wilcox rank sum test algorithm with the following parameters: ‘log_e(fold change)’ > 0.25; ‘min.pct’ > 10%; and ‘P-value’ < 0.05.

Fig. 1 Cellular heterogeneity of young inflorescence. (a) Schematic diagram of rice inflorescence development from inflorescence meristem to stamen stage used for single-cell RNA (scRNA) sequencing analysis, including S1 (< 2 mm), and S2 (2–3 mm) stages. Green colour represents leaf cells, blue colour stands for rachis cells, yellow colour indicates meristem cells, and other colours are annotated with the corresponding abbreviations: FM, floret meristem; IM, inflorescence meristem; le, lemma; lo, lodicule; pa, palea; PBM, primary branch meristem; rg, rudimentary glume; SBM, secondary branch meristem; sl, sterile lemma; SM, spikelet meristem; st, stamen. (b) Workflow for inflorescence sample collection and scRNA sequencing. The inflorescences were observed and photographed using a Leica S8APO stereomicroscope. Two replicate inflorescences at two stages (< 2 mm and 2–3 mm length) were collected, cut, and digested to form protoplasts, followed the workflow showing photographs of protoplast collection, cell capture, together with scRNA sequencing and bioinformatics analysis. Abbreviations as in (a). (c) The *t*-distributed stochastic neighbour embedding (*t*-SNE) plot of 16 clusters identified by unsupervised clustering (see the Materials and Methods section) from 37 571 inflorescence cells. Each dot denotes a single cell; colours denote cell clusters. Clusters 1 and 11 represent spikelet cells; clusters 5, 9, and 13 represent meristem cells; clusters 7, 8, 12, 14, and 15 represent leaf cells; and clusters 0, 2–4, 6, and 10 represent rachis cells. See Supporting Information Table S4 for details of enriched genes in each cluster. (d) Replicability of each of the clusters between samples as defined by the area under the receiver operator characteristic curve (AUROC) score. S1, inflorescence at < 2 mm length; S2, inflorescence at 2–3 mm length; replicates are indicated by numbers (.1, .2) after sample name. (e) Heatmap of QUSAGE gene enrichment scores of spikelet and meristem marker genes collected from published articles. Gene set activity is score calculated by QUSAGE, which means the gene set is enriched in a cluster and is probably functional. (f) Proportion of cells in each cluster from S1, S2, and young flag leaf (L) samples, showing the distinct expression profiles associated with inflorescence vs leaf tissues, and for different stages of inflorescence development. S1, inflorescence at < 2 mm length; S2, inflorescence at 2–3 mm length. (g) Gene number expressed per cell in each cluster. Boxplots show 25%, 50%, and 75% quartiles, with additional values represented by dots.

Pseudotime analysis

Single-cell pseudotime trajectories were constructed using variable genes with MONOCLE 2 with default parameters (<http://cole-trapnell-lab.github.io/monocle-release>; Qiu *et al.*, 2017). Gene expression data over pseudotime were normalized by MONOCLE 2. Based on the pseudotime analysis, branched expression analysis modelling (BEAM) was applied to genes at branch points.

Gene Ontology analysis

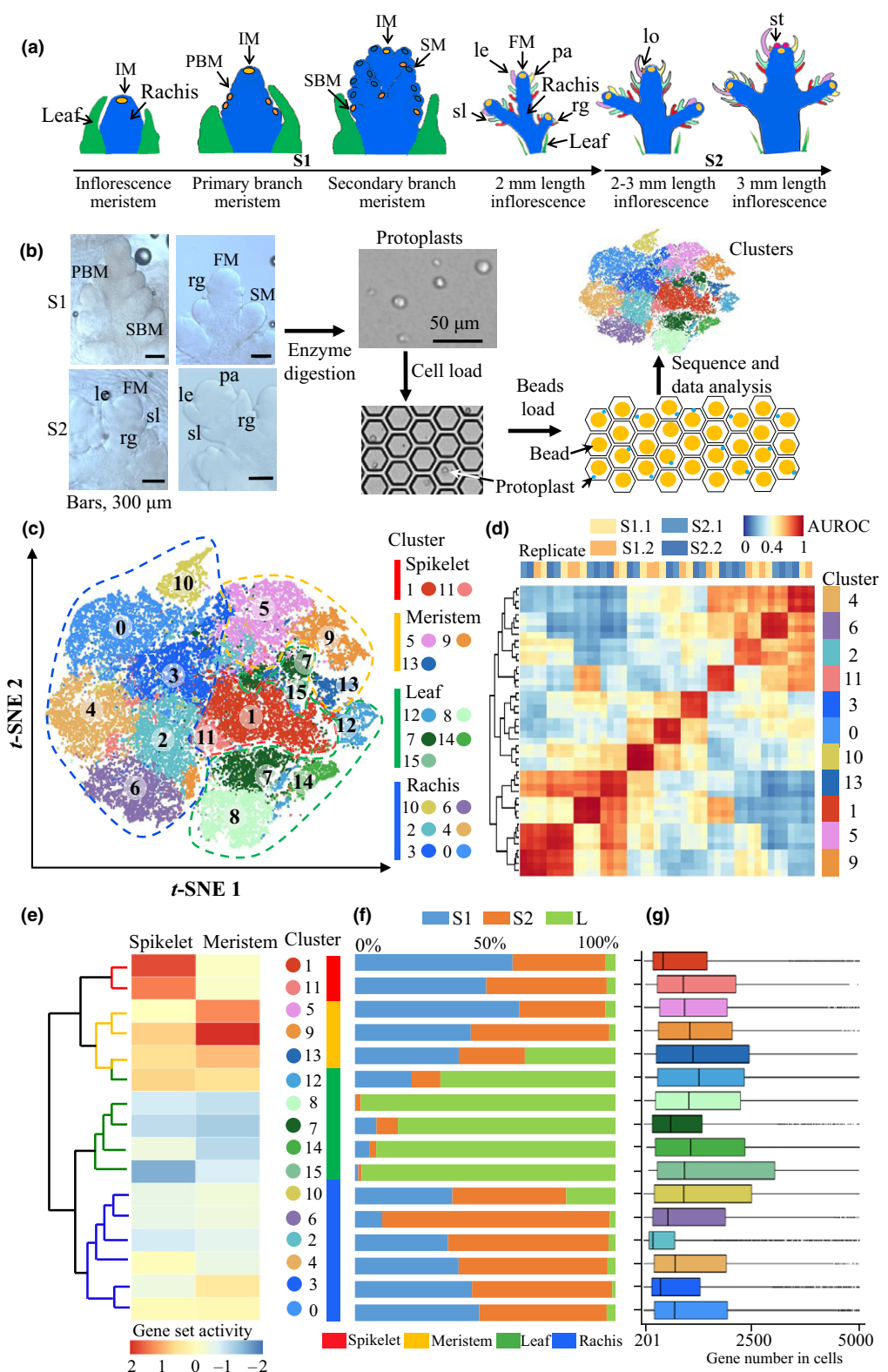
Unique genes in the significant or representative DEG profiles were assigned Gene Ontology (GO) functions to elucidate their biological functions using the R package CLUSTERPROFILER (Yu *et al.*, 2012). GO annotations were available from National Center for Biotechnology Information (<http://www.ncbi.nlm.nih.gov/>), UniProt (<http://www.uniprot.org/>), GO (<http://www.geneontology.org/>), and the Rice Genome Annotation Project (<http://rice.plantbiology.msu.edu/>). Fisher’s exact test was applied to identify the significant GO categories. *P*-value rather than false discovery rate/*P*.adjust was used as the criterion, because some GO results did not have sufficient GO terms for multiple hypothesis testing.

Quantitative set analysis for gene expression (gene enrichment) analysis

We used the QUSAGE (2.16.1) package (Yaari *et al.*, 2013) to analyse the gene expression and cluster information to characterize the relative activation of a given gene set. For cell type identity (Fig. 1e), genes from reported transcriptome data were used; for epigenetic pathway enrichment analysis, genes involved in methylation-related GO terms were used.

In situ hybridization and expression analysis

Fresh samples at the same developmental stage as for scRNA-seq were collected and fixed in FAA solution (50% ethanol, 10% formalin, and 5% acetic acid), dehydrated, infiltrated, embedded



in paraffin, and sectioned into 8 mm thick sections; subsequently, *in situ* hybridization assays were performed as previously described (Hu *et al.*, 2015). For quantitative reverse transcription

(qRT)-PCR analysis, total RNA was isolated and analysed as previously described (Hu *et al.*, 2015). All primers used for *in situ* hybridization and qRT-PCR are listed in Table S1.

Results

Single-cell transcriptomics defines discrete cell types and developmental stages in the rice inflorescence

During the transition from vegetative to reproductive development in rice, establishment of the IM, BMs, and SMs occurs within a short time window (Fig. 1a) (Ikeda *et al.*, 2004). Therefore, we collected inflorescence samples at two stages early in development – S1 (< 2 mm) and S2 (2–3 mm) – containing different tissues, including the rachis, meristems, and spikelets, before pistil primordium emergence (Fig. 1a,b). Since the bracts and inflorescence branch primordia growing at the same position cannot be removed (Ikeda *et al.*, 2004), Ls covering the inflorescence were collected as controls. In total, five samples (L and two replicates for S1 and S2) were digested for 2 h (Fig. S1a); the resulting protoplasts were transferred to the BD Rhapsody System for cDNA library preparation and scRNA-seq analyses (Fig. 1b). An average of 94 226 sequencing reads per cell was obtained (Table S3); the original data were prefiltered at both the cell and gene levels with the following exclusion criteria: low-viability cells with high mitochondria rate (mito % > 20%), and low-expressing genes ($nGene < 200$). This analysis resulted in a pool of 37 571 cells expressing 27 586 genes with an average of 4247 UMIs per cell, which could represent the transcripts captured without bias for further analysis (Fig. S1b–d; Table S3).

Unbiased clustering analyses of S1, S2, and L cells produced 16 discrete cell clusters (Fig. 1c), and the genes enriched in each cluster were identified (Fig. S1e; Table S4). The cell clusters revealed in the two replicates of S1 and S2 were highly consistent; they harboured similar cell proportions in each of the clusters (Fig. S2a), which were identified with high similarity in METANEIGHBOR analysis (Crow *et al.*, 2018), presenting as the average area under the receiver operating characteristic curve > 0.9 , except for cluster 2 (0.83) (Fig. 1d). Furthermore, their gene expression profiles were highly correlated (Fig. S2b). Some differences were observed between the two S2 samples (Fig. S2b), indicative of biological variation as inflorescence development progressed.

To assign cell identities to these clusters, we collected reported transcriptome data and marker genes that function in different cell types in inflorescence and spikelet development (Table S4) (Furutani *et al.*, 2006; Zhang & Yuan, 2014; Harrop *et al.*, 2016). Correlations between expression of marker genes and enriched genes in each cluster, defined by quantitative set analysis of gene expression (Fig. 1e) (Yaari *et al.*, 2013), assigned inflorescence clusters 1 and 11 as spikelets (composed of rudimentary glume (rg), sterile lemma (sl), and floret); and clusters 5, 9, and 13 as meristem cells (including IM, BMs, and SM). For the remaining clusters, leaf (clusters 7, 8, 12, 14, and 15) or rachis (clusters 0, 2–4, 6, and 10) cell identity was assigned based on the predominance of genes from either the L or S1/S2 samples, respectively (Figs 1c,f, S1f, S2d).

These four cell types (spikelet, meristem, rachis, and leaf) exhibited distinct expression profiles (Fig. S1e) and were enriched with distinct GO biological functions (Table S5). E-class gene *OsMADS1* and cytokinin-activating enzyme *LONELY GUY* were enriched in the spikelet and the meristem cluster, respectively (Fig. S1e;

Table S4), whereas genes associated with ‘water transport’ and ‘xylem development’ processes and those related to ‘photorespiration’, ‘response to water deprivation’, ‘glycolytic process’, ‘gluconeogenesis’, and ‘water transport’ processes were enriched in rachis and leaf cluster, respectively (Table S5). All three sample types (S1, S2, and L) had a unique profile of cells within each cluster (Figs 1f, S1e, f). Both inflorescence samples and all clusters contained leaf-identity cells (Figs 1f, S2d). Cells in cluster 13 contained a high proportion of leaf-identity cells, which may represent cells that are differentiating into leaf cells from the meristem. Cells in cluster 10 contained a high proportion of leaf cells, which may reflect parenchyma tissues that exist in all tissues (Fig. 1f). Cluster 2 harboured the fewest expressed genes, indicating likely mature cells expressing a limited number of genes (Fig. 1g; Table S5).

A developmental transition was observed between S1 and S2 samples. More meristem cells were present in S1 than in S2 samples (Fig. 1f), confirming that S1 samples were earlier than S2 samples at their developmental stages. Conversely, more rachis cell types were present in S2 samples (Fig. 1f), indicating that S2 samples were later than S1 samples at their developmental stages, where rachis/branch elongation accelerates (Ikeda *et al.*, 2004). Genes related to ‘response to stress’, ‘cell division’, and ‘DNA methylation’ were enriched in meristem cell clusters 5 and 9 (Table S5), whereas genes related to ‘flower development’, ‘response to hydrogen peroxide’, and ‘regulation of cell cycle’ were enriched in spikelet cell clusters 1 and 11 (Table S5), consistent with the developmental trajectory from meristem maintenance to floral organ specification (Fig. 1a). These results reveal that a high degree of cell heterogeneity exists in early rice inflorescences and that scRNA-seq-derived transcriptome data can facilitate the identification of discrete cell types and developmental stages in rice inflorescence.

Spikelet cell clusters can be classified based on gene expression profiles

A second subclustering analysis using inflorescence clusters 1 and 11 revealed 10 spikelet subclusters, with clear hierarchical structures when presented with the UMAP algorithm (Fig. 2a) (Jean-Baptiste *et al.*, 2019; Zhang *et al.*, 2019). *DWT1*, encoding the WUSCHEL-related homeobox (WOX) TF expressed in young panicles and FMs (Wang *et al.*, 2014), was specifically enriched in spikelet subcluster 7, suggesting that cells in this subcluster are FM cells (Fig. 2b).

The cell identities of these spikelet subclusters were determined by enriched expression of spikelet marker genes (Fig. 2b; Table S4). Specific enrichment of *DWT1* and E-class genes *OsMADS6* and *OsMADS8* in spikelet subclusters 7 and 5, respectively, identified these two subclusters as flower cells, revealing their distinct developmental trajectory, whereas enrichment of *OsMADS1* in spikelet subcluster 0 indicated its lemma identity (Fig. 2b).

Identification of the close connection of all spikelet subclusters allowed us to construct a developmental trajectory of spikelet cell differentiation over pseudotime (Fig. 2a,c) (Qiu *et al.*, 2017). Cells from spikelet subclusters 1, 3, and 6 were evenly distributed in all developmental trajectories (Fig. 2c),

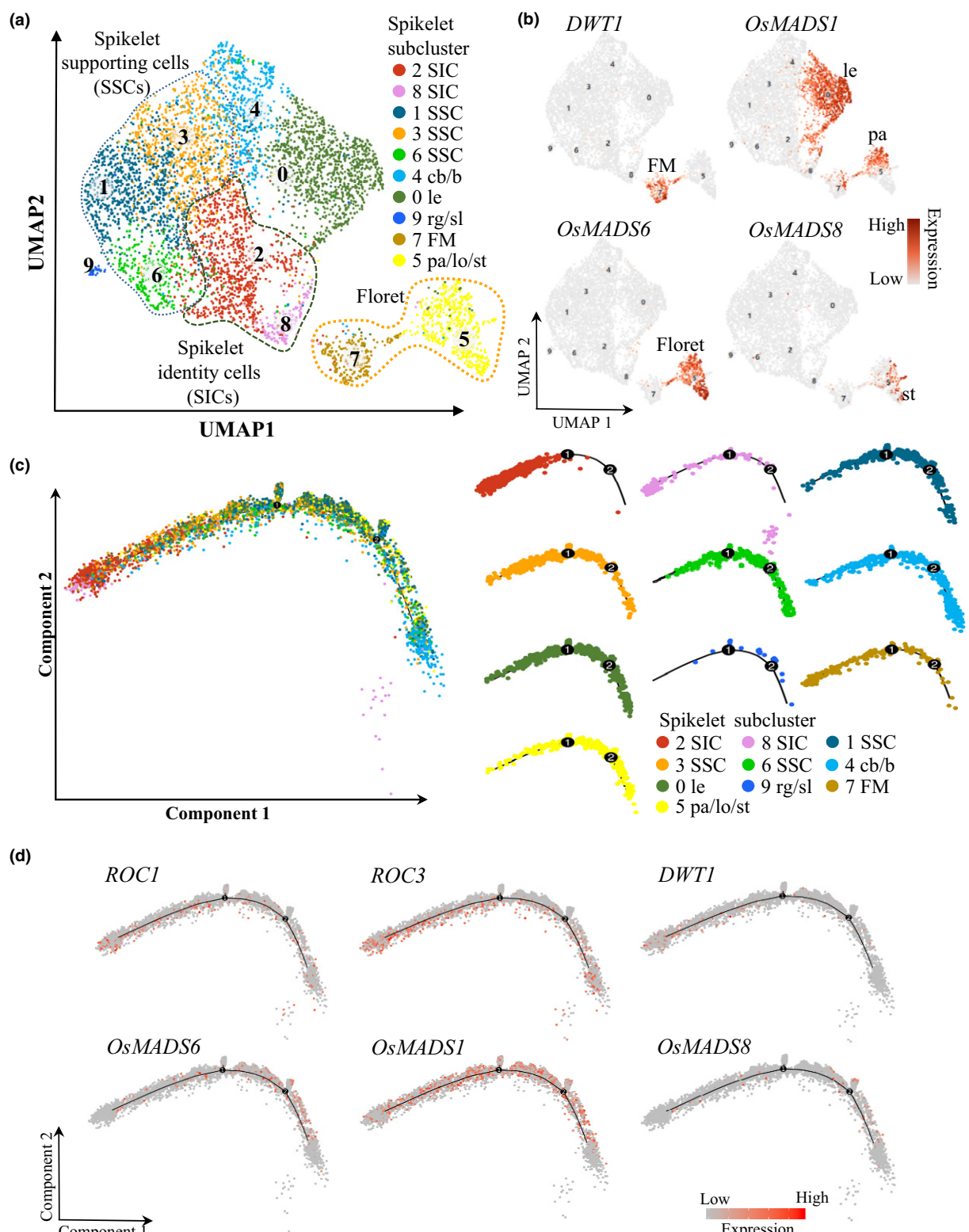


Fig. 2 Cell type identification and pseudotime trajectories in all spikelet cells in rice. (a) Uniform manifold approximation and projection (UMAP) plot of unbiased reclustering of the 5217 spikelet cells (clusters 1 and 11, Fig. 1c), revealing 10 subclusters that identified spikelet supporting cells (SSCs), spikelet identity cells (SICs), and floret cells. Red line indicates reproductive (floral) developmental trajectories of spikelet cells. le, lemma; cb/b, cryptic bract/bract; pa/lo/st, palea/lodicule/stamen; FM, floret meristem; rg/sl, rudimentary glume/sterile lemma. (b) Feature plots for marker genes expression based on (a). Abbreviations as in (a). (c) Pseudotime analysis using all spikelet subclusters to show the developmental process of spikelet development. Coloured dots and pie indicate cells from clusters in (Fig. 2a). Abbreviations as in (a). (d) Expression patterns of six spikelet marker genes are shown over the course of pseudotime.

and their gene expression profiles were enriched for 'cell cycle', 'response to stress', and 'response to abiotic stimulus' (Table S5). Therefore, they were classified as spikelet supporting cells (SSCs) underpinning overall spikelet development

(Fig. 2a). Cells from spikelet subclusters 2 and 8 were grouped at one end of the branch and cells from subcluster 5 were grouped at the other end (Fig. 2c), showing specific expression patterns of flower marker genes (Fig. 2d). Cells from spikelet

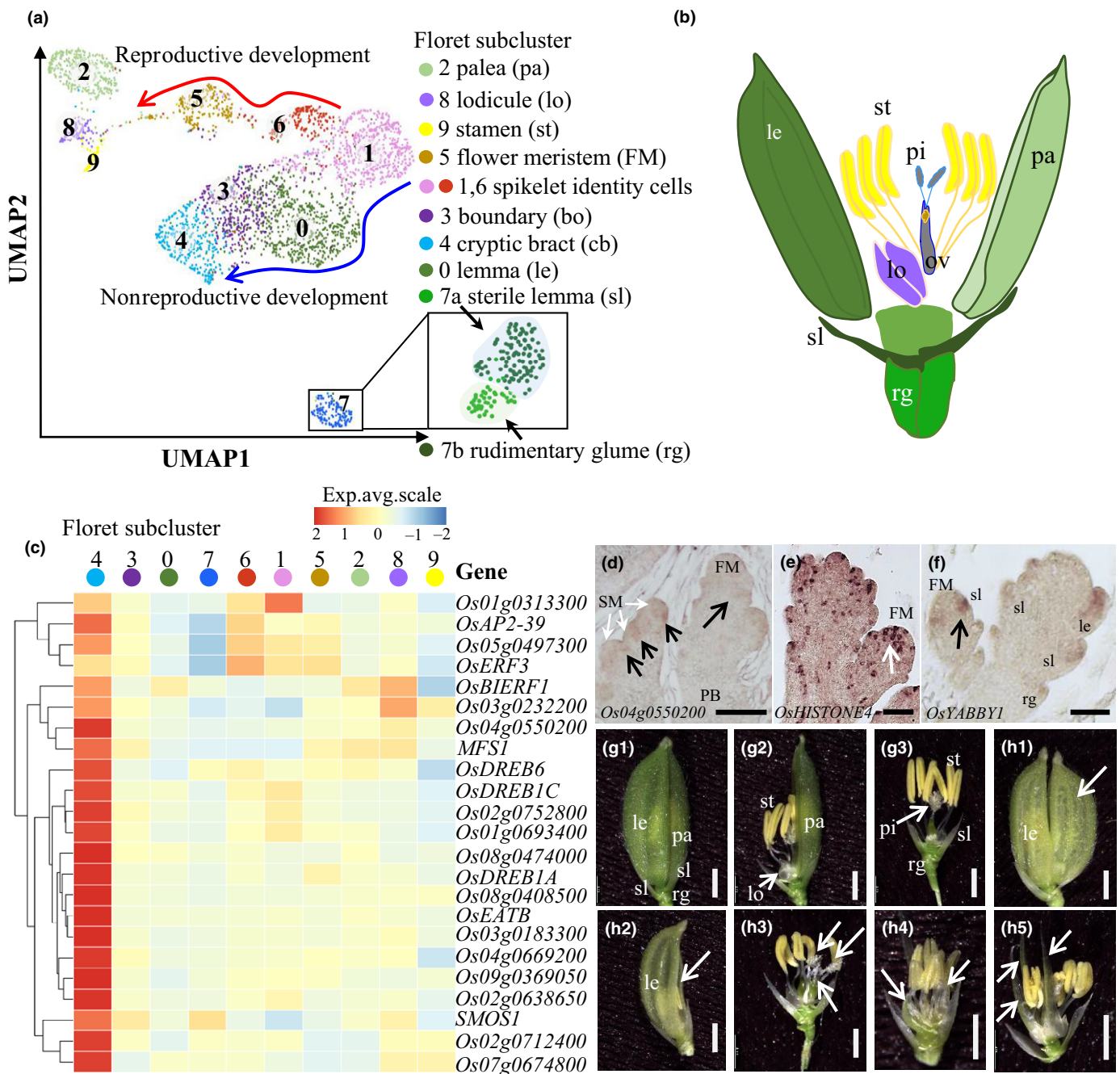


Fig. 3 Reconstruction of floret cell identity and differentiation trajectory of floret organs in rice. (a) Uniform manifold approximation and projection (UMAP) plot of unbiased reclustering of spikelet clusters 1 and 11 after removal of spikelet supporting cells, revealing 10 floret cell subclusters. Red and blue arrows indicate reproductive (floral) and nonreproductive (lateral organ) developmental trajectories of floret cells, respectively. (b) Schematic illustration of spikelet and floret structure. ov, ovule; pi, pistil. Other abbreviations as in (a). (c) Heatmap of expression of genes encoding APETALA2/ETHYLENE RESPONSE FACTOR transcription factors by floret subcluster, showing higher expression in cryptic bract cells (floret subcluster 4). Gene expression is averaged scaled value (Exp.avg.scale). (d–f) *In situ* hybridization of (d) *Os04g0550200*, (e) *OsHISTONE4*, and (f) *OsYABBY1* messenger RNAs (mRNAs). Arrows indicate high levels of mRNA accumulation. Bar, 50 µm. SM, spikelet meristem; PB, primary branch. Other abbreviations as in (a). (g) Phenotype of wild-type cv 9522 spikelet, showing (g₁) palea, lemma, sterile lemmas, and rudimentary glumes, (g₂) lodicule and stamen, and (g₃) pistil. Abbreviations as in (a). Bar, 2 mm. (h) Phenotype of *dwarf tiller1* spikelet and floret. Arrows indicate (h₁) abnormal palea or (h₂) missing palea, (h₃) multiple pistils, and (h₄, h₅) elongated, glume-like lodicules. Abbreviations as in (a). Bar, 2 mm.

subclusters 2 and 8 with similar gene expression profiles and GO gene annotations (Table S5) shared a similar pseudotime developmental trajectory as subcluster 7 with meristem identity (Fig. 2c); both were classified as spikelet identity cells (SICs). In sum, the pseudotime analysis of spikelet subclusters revealed three possible developmental branches: FM-SSC, FM-SIC, and FM-floret; the last one will be analysed in the following.

Single-cell RNA sequencing discovers role of *DWT1* in FM activity maintenance and palea specification

To specifically examine floret development, we removed SSC subclusters and reclustered the remaining cells into 10 floret cell subclusters, which could be assigned to all known floral organs (Figs 3a,b, S3b). Floret subclusters 1 and 6 were assigned as SICs, since cells in these two clusters overlapped with spikelet subclusters 2 and 8 (Fig. S3a). Floret subclusters 0, 2, 8, and 9 were assigned as lemma, palea, lodicule, and stamen, respectively (Fig. S3b).

Several floret subcluster-specific expression profiles were observed (Fig. S4a; Table S4). The enrichment of AP2/ERF TFs in floret subcluster 4 (Fig. 3c) – confirmed by *in situ* hybridization analysis of *Os04g0550200* that encodes an AP2/ERF TF – revealed its specific transcription in cells on the abaxial side of SM and FM (Fig. 3d). As *Arabidopsis* mutants of AP2/ERF TF exhibited cryptic bracts (Karim *et al.*, 2009; Chandler & Werr, 2017) and rice mutants of AP2/ERF TF, *mfs1*, showed multiple glume-like organs (Ren *et al.*, 2013), floret subcluster 4 was classified as ‘cryptic bract’ cells. Genes encoding histones were enriched in floret subclusters 3 and 4 (Table S4), and *Histone4* transcripts also accumulated in cells adjacent to SM and FM (Fig. 3e), suggesting a possible conservative bract suppression during rice flower development, whose production would otherwise compete with meristems (Chandler, 2012). Correspondingly, floret subcluster 3 was classified as ‘boundary’ cells, separating SICs and lemma from cryptic bract cells (Fig. 3a).

Floret subcluster 7 was discrete from the main cell clusters (Fig. 3a), with enriched expression of *OsMADS1*, *DL*, and *YABBY* genes. Expression of *OsYAB1* (also known as *TOBI*) was detected specifically in the lateral organs, including rudimentary glume, sterile lemma, and lemma (Figs 3f, S3b,c), which corroborated previous reports of the role of *OsYABBY*TFs in separating spikelet from meristem identity (Tanaka *et al.*, 2012, 2017). Combined with enriched expression of *OsMADS1*, *OsMADS6*, and *DL* (Table S4), this subcluster was further divided into 7a (sterile lemma) and 7b (rudimentary glume; Figs 3a, S3c).

DWT1 controls internode elongation and synchronizes the development of tillers and the main shoot (Wang *et al.*, 2014), but there has been no report on its function in flower development. We further functionally characterized the role of *DWT1* in floret development because *DWT1* was specifically enriched in floret subcluster 5 (FM; Fig. S3b). Analysis of *dwt1* florets (Wang *et al.*, 2014) revealed that most (two out of three) *dwt1* florets had identical floret structure to wild-type plant, exhibiting a structure of two rudimentary glumes, two sterile lemmas, and one floret, each with one lemma, one palea, two lodicules, six stamens, and one pistil (Figs 3g, S4b,c), whereas the remaining (one out of three) *dwt1* spikelets exhibited one of two

classes of mutant phenotype: type I mutants had a palea that grew like a lemma, and type II had no palea at all (Figs 3h, S4b,c). Both types I and II *dwt1* florets also grew multiple glume-like organs and had fewer stamens (five) and occasionally two pistils (Figs 3h, S4b,c). Mutant phenotyping data indicated that *DWT1* participated in flower development, regulating FM activity and palea development.

Single-cell RNA sequencing provides new insights into rice floret specification pathways

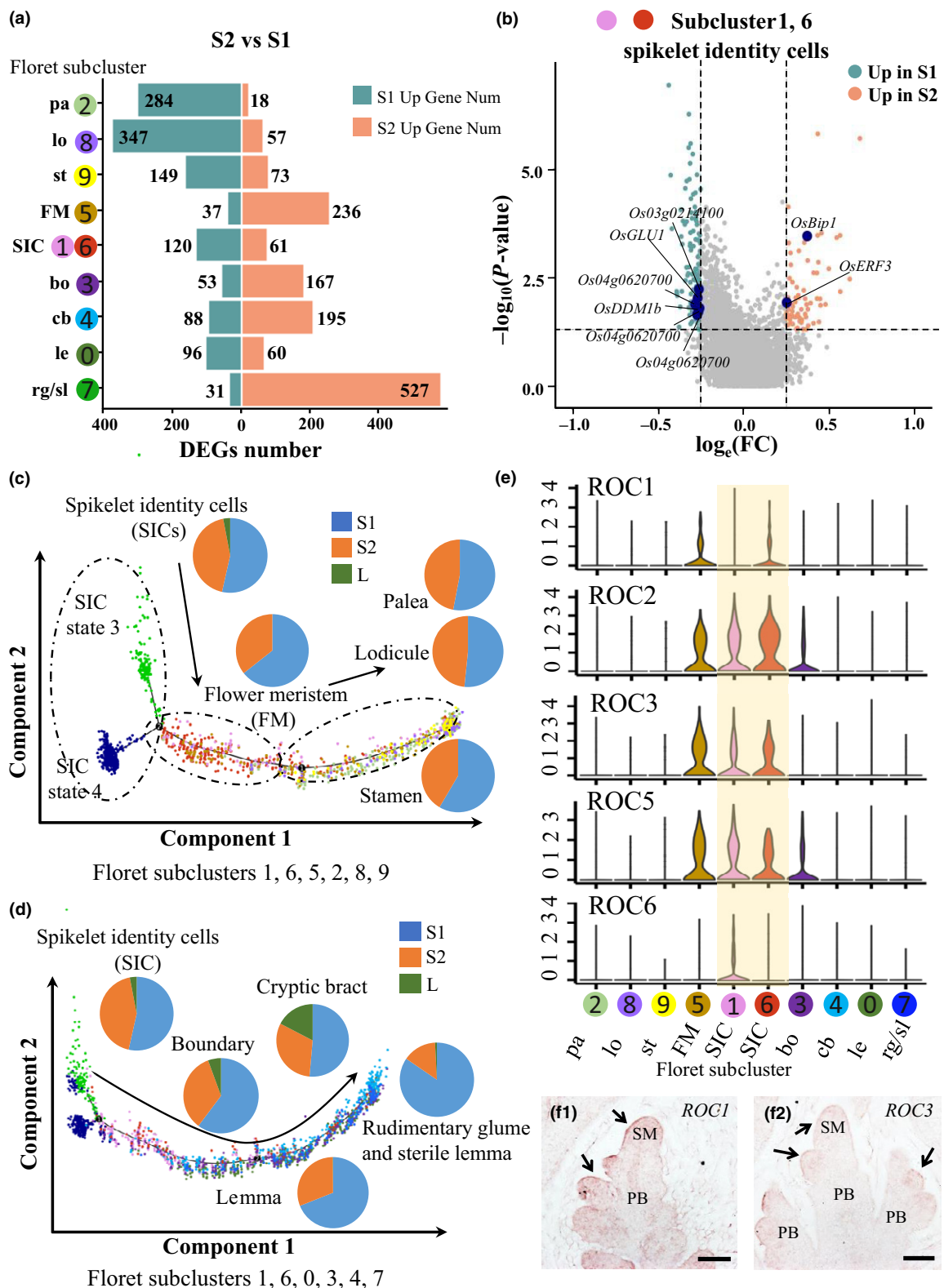
To further identify putative regulatory genes and pathways in floral organ specification, we examined floret subclusters for DEGs between S1 and S2 stages and revealed 2194 DEGs across the 10 subclusters (Fig. 4a; Table S6). In floret subcluster 5 (FM cells), genes involved in signal transduction, including *FLR1* (Li *et al.*, 2016), *OsFLS2* (Wang *et al.*, 2015b), and *RGB1* (Sun *et al.*, 2014, 2018), were highly upregulated in S1 (Table S6), suggesting that a *FLR1/OsFLS2–RGB* module-mediated immune response likely regulates rice FM activity, as it does in maize (Wu *et al.*, 2020).

Genes previously implicated in meristem maintenance and initiation, adaxial/abaxial pattern specification, programmed cell death, and cell cycle, such as *OsPNH1* (Nishimura *et al.*, 2002), rice *HOMEODOMAIN CONTAINING PROTEIN4* (*OSHB4*; Y. Y. Li *et al.*, 2016), and *OSH71* (Kuijt *et al.*, 2014), were associated with floret subcluster 4 (cryptic bract cells; Table S6) [Correction added after first publication 24 February 2022: a reference has been deleted from the preceding sentence]. Considering their high correlations with cell activity, we propose that these cells are specialized cells for polarity establishment. Similarly, genes involved in cell growth, such as *OsCCS52A1* (also known as *TAD1* and *TE*, Table S6) (Lin *et al.*, 2012; Su’udi *et al.*, 2012; Xu *et al.*, 2012), were upregulated in S2 floret subcluster 3 (boundary cells), suggesting roles of floret subcluster 3 in organ separation.

Genes and processes involved in epigenetic regulation, including DNA methylation and histone modification, were also enriched in floret cell subclusters (Table S7), suggesting that changes at the genomic level accompany the cellular transition to reproductive development in different floret cell types. Consistently, various active histone modifications and a global *de novo* DNA methylation were found to play a crucial role for rice reproductive development (Higo *et al.*, 2020; Zheng *et al.*, 2021; Wang *et al.*, 2022).

Floret developmental trajectory reconstruction reveals floret organ identities

Two continuous developmental trajectories were revealed in the UMAP of floret cells, representing flower development and lateral organ differentiation events (Fig. 3a). Since scRNA-seq enables the reconstruction of a continuous differentiation trajectory of a developmental process (Zhang *et al.*, 2019, 2021a), pseudotime analyses were constructed using floret subclusters along each trajectory (Fig. 4c,d). Two clusters of cells inferred at the beginning of pseudotime in both analyses, named SIC states 3 and 4 (Fig. 4c,d), overlaying these cells onto the floret



subcluster UMAP confirmed that they belong to SICs (floret subclusters 1 and 6; Fig. S4d). Enriched genes in SIC states 3 and 4 were involved in 'cell defence' and 'intracellular signal transduction' GO processes (Table S5). Among them were the genes encoding homeobox-leucine zipper RICE OUTERMOST

CELL-SPECIFIC (ROC) TFs (Fig. 4e) (Ito *et al.*, 2003). In *Arabidopsis*, *HOMEODOMAIN GLABROUS* (*HDG*), homologous of *ROC* genes, are expressed specifically in the epidermis (Horstman *et al.*, 2015); in rice, *ROCs* increase spikelet size and number (Zou *et al.*, 2011), which were prominently expressed at

Fig. 4 Reconstruction of floret cell identity and differentiation trajectory of floret organs in rice. (a) Differentially expressed genes (DEGs) in all floral subclusters. Number on bar indicates the number of DEGs in each cluster. DEGs defined as fold change (FC) >1.28 ($|\log_e \text{FC}| > 0.25$) and $P < 0.05$. Because S1 and S2 were very close developmental stages with a relatively small number of DEGs, we chose $|\log_e \text{FC}| > 0.25$ (SEURAT default parameter) instead of $\text{FC} > 2$, and use P -value instead of false discovery rate FDR to find DEGs. pa, palea; lo, lodicule; st, stamen; FM, flower meristem; SIC, spikelet identity cell; bo, boundary; cb, cryptic bract; le, lemma; rg, rudimentary glume; sl, sterile lemma. (b) Volcano plots of gene expression in subclusters 1 and 6 of floret genes. DEGs upregulated in S1 tissues are marked in blue; DEGs upregulated in S2 tissues are marked in orange; labelled genes marked with large navy-blue dot. More detail information can be found in Supporting Information Table S6. (c, d) Pseudotime analysis using floret subclusters, showing that (c) FM cells are transitional cells that develop floral organs, including palea, lodicule, and stamen; and (d) FM cells also differentiate into glumes, cryptic bract, and boundary cells. Pie plots represent the cell percentage in S1 and S2 samples. Two subsets of floret SIC subclusters 1 and 6, labelled here as SIC states 3 and 4 in green and navy-blue, respectively, denote the beginning of pseudotime (also see Fig. S4d); arrows indicate progress through pseudotime. Coloured dots indicate cells from clusters in Fig. 3a. (e) Violin plots showing expression pattern of selected RICE OUTERMOST CELL-SPECIFIC (ROC) genes in floret subclusters. Abbreviations as in (a). (f) *In situ* hybridization of (f₁) ROC1 and (f₂) ROC3 messenger RNAs (mRNAs). Arrows indicate high levels of mRNA accumulation in the L1 layer. Bar, 50 μm . SM, spikelet meristem; PB, primary branch.

the beginning point in the developmental trajectory of spikelets (Fig. 2d). Therefore, these cells could be on the FM surface to respond to environmental signalling and affect lateral organ specification. Consistent with their distinct enrichment patterns (Fig. 4e), expression signals of *ROC1* and *ROC3* were especially detected in the L1 layer of inflorescence (Figs 4f, S4e,f).

Though the SIC floret subclusters contained cells with leaf identity, none of the floral organs that developed from these SICs over pseudotime, including the FM, palea, lodicule, or stamen, contained cells with leaf identity (Fig. 4c). In the lateral organ trajectory, five organs differentiated from SICs all contained cells with leaf-like identity (Fig. 4d), suggesting that these organs possess an intermediate identity between nonreproductive leaves and reproductive floral organs. These floret developmental trajectories provide clear cellular evidence that the ‘true’ rice flower develops in a SIC–FM–palea/lodicule/stamen pattern with organs distinct from leaves, whereas the lemma, rudimentary glume, and sterile lemma are likely to be bract-like organs that subtend the flower with intermediate leaf/flower organ identity.

Subclustering reveals three different inflorescence meristem types

The same strategies were applied to more closely examine 5611 meristem cells in inflorescence clusters 5, 9, and 13; unbiased reclustering yielded 12 meristem subclusters (Figs 5a,b, S2c, S5a; Tables S4, S5). IM and SM marker genes were used to assign cell types to subclusters (Table S4), but most marker genes could not distinguish between heterogeneous meristem cell types because they were widely expressed in all meristem subclusters (Fig. S5b).

However, some marker genes with reported functions in IMs and SMs exhibited cluster-specific expression and could be used to categorize meristem subclusters into three groups: IM, BM (comprising PBM, ePBM, and SBM), and SM (Figs S2c, S5c, S6a) (Furutani *et al.*, 2006; Harrop *et al.*, 2016). Along with the UMAP plot (Fig. 5a), these identities could be used to classify meristem subclusters as IM (subclusters 0, 1, 5, 9, 11), BM (3, 4, 6–8), and SM (2, 10) (Fig. 5b). These categorizations also explained why SM cluster (inflorescence subcluster 13) had many cells with a leaf identity, since the nonreproductive floret organs with leaf-like identity, including rudimentary glume, sterile lemma, and lemma, are generated from SM (Wu *et al.*, 2018).

Genes enriched in IM cells were involved in ‘regulation of meristem growth’, ‘response to wounding’, ‘stem cell population

maintenance’, and ‘response to auxin’ (Figs 5b, S6b; Table S5), providing a valuable meristem candidate gene pool for further validation and agricultural application.

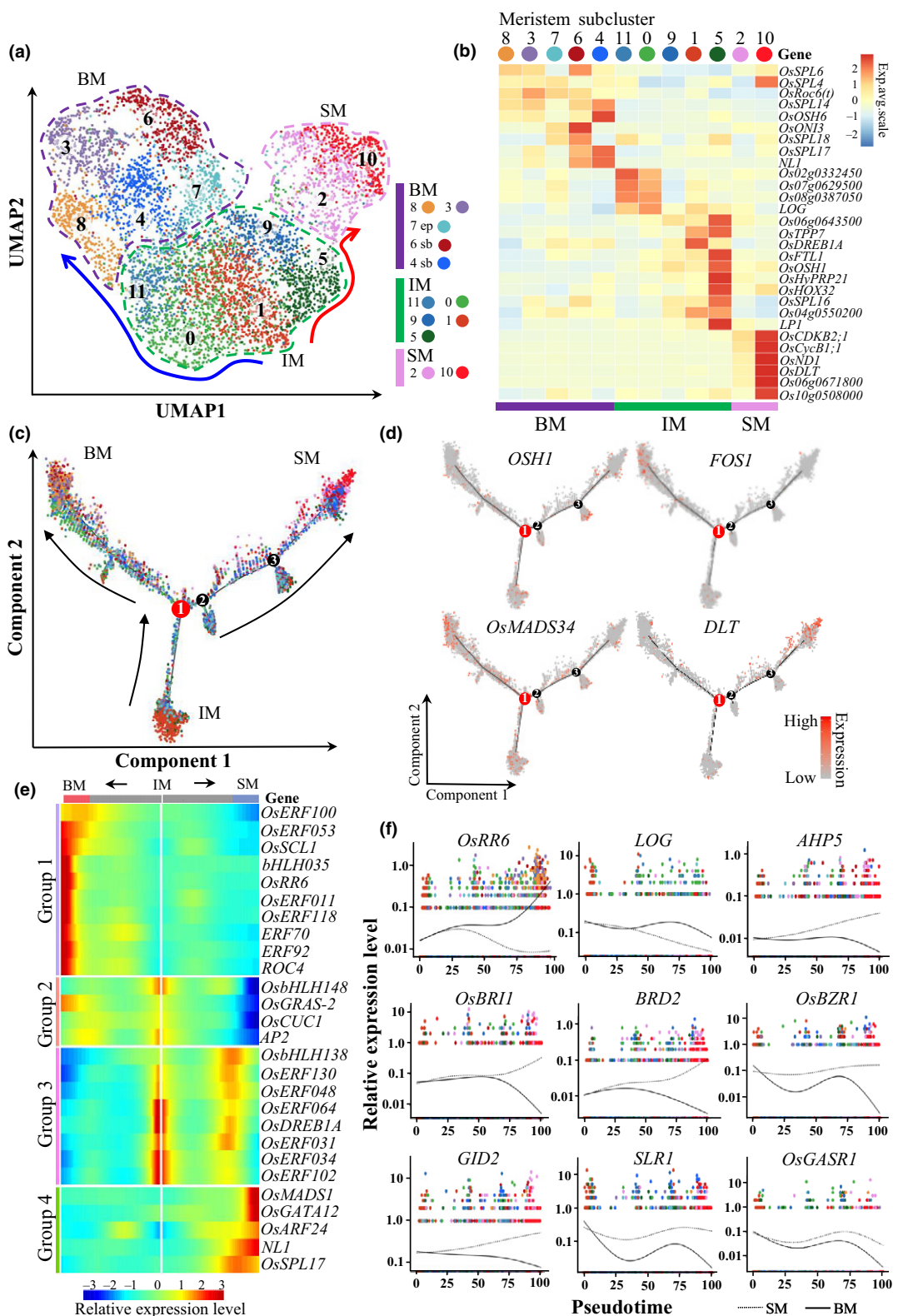
Each of these meristem types contains cells from multiple subclusters, confirming high levels of heterogeneity in reproductive meristem cells. Genes encoding TFs that regulate inflorescence branching, including WOX, OSH, ROC, SPL, and YABBY members, displayed distinct expression patterns in each subcluster (Fig. S6c) and were consistent with those reported in the literature (Jiao *et al.*, 2010; Miura *et al.*, 2010; Wang *et al.*, 2015a; Q. L. Wang *et al.*, 2018; Yuan *et al.*, 2019) [Correction added after first publication 24 February 2022: a reference has been deleted from the preceding sentence]. However, specific identities of each meristem subcluster remain open for further studies.

ROC family genes, as well as genes annotated with ‘response to chitin’, were enriched in meristem subcluster 7 (Table S5), suggesting that meristem subcluster 7 could be epidermal cells. Indeed, most maize *ZmHDZIV* genes, which are homologues of *ROC* genes, express preferentially in the epidermis (Javelle *et al.*, 2011). Furthermore, considering that *OsLTPG2* (Os03g0167000) and *ONI1* (Os03g0181500), orthologues of maize GRMZM5G850455 and GRMZM2G445602 listed as maize meristem epidermal marker genes, respectively (Xu *et al.*, 2021), were also enriched in meristem subclusters 6 and 7 (Fig. S6a), which were assigned as epidermis cells.

Expression analysis revealed 448 DEGs in meristem subclusters, mostly associated with environmental responsiveness, including salt, temperature, oxygen, and stress responses (Tables S4, S6). Of these, reactive oxygen species have been linked not only to stress response, but also to control of cell cycle and meristem development (Schippers *et al.*, 2016; Yang *et al.*, 2018). Although another possibility is that protoplast digestion may induce the expression of stress-responses-related genes. Genes involved in epigenetic modification pathways were specifically activated in the SM (Table S7), suggesting that changes in genomic regulation and protection accompany meristem transition (Higo *et al.*, 2020; Satterlee *et al.*, 2020) and may prepare the plant for floret initiation.

Reproductive meristem development responds to transcription factor and phytohormone signals

The UMAP plot of meristem cell subclusters demonstrated that two differentiation events likely exist in rice reproductive



meristem development (Fig. 5a). Accordingly, the pseudotime progression began with IM subclusters and ended at either BM or SM subclusters through branch point 1 (Figs 5c, S7a,b).

Meristem marker genes *OSH1* and *FOS1*, which had been enriched in IM and BM, respectively (Fig. 5b) (Suzuki *et al.*, 2009; Tsuda *et al.*, 2011), appeared to function independently in

Fig. 5 Reconstruction of meristem cell identity and differentiation trajectory of inflorescence meristems in rice. (a) Uniform manifold approximation and projection (UMAP) plot of unbiased reclustering of meristem clusters 5, 9, and 13, revealing 12 meristem cell subclusters. Clusters could be classified into three cell types: BM, branch meristems including the primary branch meristem, elongated primary branch meristem, and secondary branch meristem; SM, spikelet meristem; and IM, inflorescence meristem. Red and blue arrows indicate SM and BM developmental trajectories of meristem cells, respectively. ep, epidermis; sb, suppressed bract. (b) Heatmap of marker gene expression in meristem subclusters. Abbreviations as in (a). (c) Pseudotime analysis using meristem cells to show the developmental trajectory of meristem differentiation, from IM into BM or SM. Coloured dots indicate cells from clusters in (a). Numbers in circles indicate branch points in the developmental trajectories; red circle indicates the branch point analysed in (e). Abbreviations as in (a). (d) Feature plots for expression of four genes based on (c). (e) Heatmap showing expression of genes encoding transcription factors selected from the first branch point in meristem cells over pseudotime (point 1 in (c)). The white line in the middle represents the beginning of pseudotime (IM); the two sides represent the ends of pseudotime down the two lineages (left, BM; right, SM). The gene expression level is scaled and relative to the mean value of one gene. Abbreviations as in (a). (f) Scatter plot based on branched expression analysis modelling of hormone-related genes. Coloured dots indicate cells from clusters in (a). Abbreviations as in (a).

maintaining SM and BM activity, respectively (Fig. 5d). Expression of *OsMADS34*, which regulates rice inflorescence branching (Gao *et al.*, 2010; Kobayashi *et al.*, 2010), was enriched in the IM and appeared to peak in the middle of pseudotime, whereas expression of *DLT*, which controls inflorescence elongation (Hirano *et al.*, 2017), peaked in two waves in BM, with a general increase during SM development (Fig. 5d).

BEAM was applied to the top 1000 HVGs at branch point 1 during meristem differentiation. Four groups of genes emerged (Table S6), all of them containing various TFs known to be involved in inflorescence development (Fig. 5e). Expression levels of group 1 genes increased in the BM pathway but remained stable or decreased in the SM pathway, and they were generally involved in environmental and stress responses (Fig. S7c). Group 1 also contained *OsRR6*, a CK-inducible gene whose over-expression reduces branch number and shortens the inflorescence (Hirose *et al.*, 2007); thus, group 1 genes might be involved in primary branch elongation.

Group 2 and group 3 genes appeared to be involved in promoting meristem transition from IM to BM and SM, respectively. Expression levels of group 2 genes decreased significantly in the SM pathway, whereas those levels in the BM pathway remained relatively constant over pseudotime. Group 3 genes were expressed highly in the IM pathway but significantly lower in the BM pathway; in the SM pathway, expression levels of group 3 genes initially reduced, but they peaked again before the final differentiation into SM (Table S6).

In contrast to group 1, expression levels of group 4 genes increased in the SM pathway (Fig. S7c); they encoded genes involved in cell cycle and epigenetic processes. *NECK LEAF1* (*NL1*), encoding a GATA-type zinc finger TF, was enriched in BM (Fig. 5b) and controls fate transition to SM (Fig. 5e). *NL1* expression is localized in suppressed bract cells (Wang *et al.*, 2009), a specialized inflorescence zone with meristem identity similar to the floret region that regulates primary branch and spikelet numbers (Wang *et al.*, 2009; Lu *et al.*, 2017), allowing us to classify meristem subclusters 4 and 6 as suppressed bract cells (Fig. 5a,b). Indeed, the *miR156/529-SPL* module coordinates with *NL1* in suppressing bract growth and activating transition from vegetative to reproductive branching (Wang *et al.*, 2021).

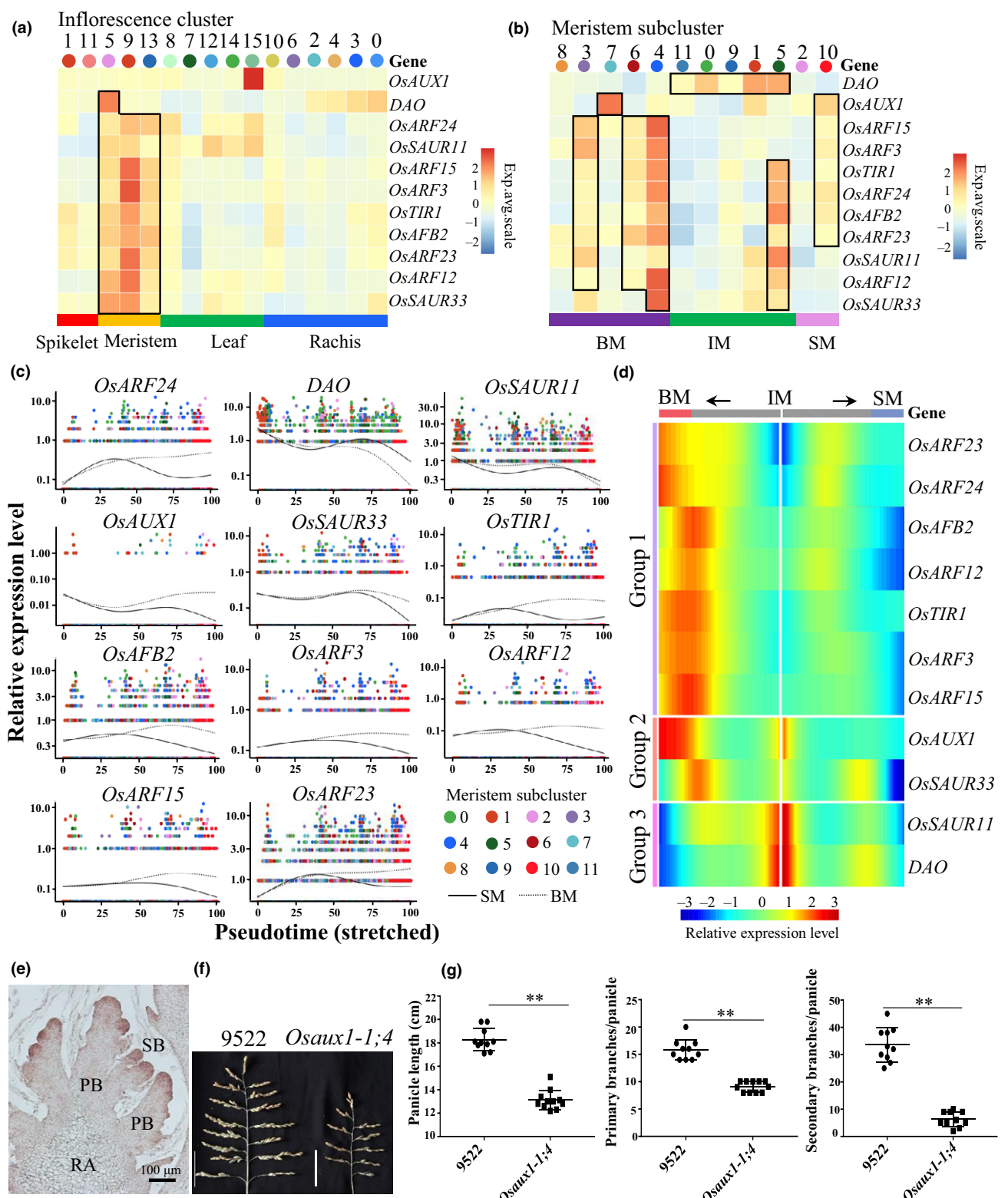
Genes encoding components in phytohormone signalling pathways, including CK, auxin, brassinosteroids, and GA

(Wils & Kaufmann, 2017; Yuan *et al.*, 2020; Zhu & Wagner, 2020), were also expressed in discrete patterns over the two differentiation trajectories. Indeed, genes related to biosynthesis or signal transduction of these hormones show switch-like patterns leading to gradual transition from IM to BM or SM development, respectively (Fig. 5f), supporting the series of pattern shifting during rice inflorescence development (Kyozuka *et al.*, 2014).

OsAUX1 promotes primary branch elongation and spikelet initiation

Auxin is one of the most important phytohormones in regulating meristem initiation in *Arabidopsis*, maize, and *Setaria viridis* (Yuan *et al.*, 2020; Zhu & Wagner, 2020), but there is very little direct genetic evidence for its role in rice inflorescence development. One exception is that mutation of *FISH BONE*, the orthologue of *TRYPTOPHAN AMINOTRANSFERASE OF ARABIDOPSIS* that encodes an enzyme involved in auxin biosynthesis, showed small inflorescences (Yoshikawa *et al.*, 2014). We examined the expression of genes involved in auxin biosynthesis, transport, and signal transduction in identified inflorescence clusters and meristem subclusters (Fig. 6a; Table S4). Genes encoding auxin-responsive TFs and auxin receptors exhibited similar expression patterns in both inflorescence clusters and meristem subclusters. *DIOXYGENASE OF AUXIN OXIDATION* (DAO), involved in auxin catabolism, was specifically expressed in IM clusters and meristem subclusters, and *OsAUX1*, an auxin influx transporter, was enriched in inflorescence cluster 15, meristem subcluster 7, and meristem subcluster 10 (Fig. 6a,b). Most auxin pathway genes exhibited similar switch-like patterns in SM or BM identity transition as group 1 genes over meristem pseudotime, although *DAO*, *OsAUX1*, and two *S*mall *A*UXIN-*U*PREGULATED RNA TF-encoding genes belonged to different groups (Fig. 6c,d). Hence, the role of *OsAUX1* in inflorescence development was further investigated.

OsAUX1 facilitates primary root and root hair elongation in response to phosphate and cadmium stress (Yu *et al.*, 2015; Giri *et al.*, 2018), but its role in inflorescence development remains unclear. *In situ* hybridization confirmed that *OsAUX1* was expressed in BM and SMs (Figs 6e, S8a), which was consistent with the scRNA-seq analysis (Fig. 6b). Both the CRISPR-Cas9-edited mutant *Osaux1-1;4* and the transfer DNA insertion



mutants (Giri *et al.*, 2018) *Osaux1-1;1* and *Osaux1-1;3* produced shorter inflorescences with fewer branches and spikelets (Figs 6f, g, S8b–d). These results indicated that *Osaux1* plays a pivotal role in controlling meristem determinacy during rice inflorescence development.

Dynamic distribution pattern of *OsMAPK6* and *OsGASR1* determines inflorescence architecture

To further validate our cluster and cell-type annotations, we analysed dynamic expression of *OsMAPK6*, a key member in the

Fig. 6 The role of auxin-related genes in meristem cell development in rice. (a) Heatmap showing expression of auxin-related gene in all cell types (16 clusters). (b) Heatmap showing expression of auxin-related genes in meristem cell subclusters. BM, branch meristems including the primary branch meristem, elongated primary branch meristem, and secondary branch meristem; SM, spikelet meristem; IM, inflorescence meristem. (c) Scatter plot based on branched expression analysis modelling of auxin-related genes. (d) Heatmap showing expression of auxin-related genes in meristem cells over branch point 1 of pseudotime (see Fig. 5c). The white line in the middle represents the beginning of pseudotime (IM); the two sides represent the ends of pseudotime down the two lineages (left, BM; right, SM). Abbreviations as in (b). (e) *In situ* hybridization of *OsAUX1* in S1 inflorescence. PB, primary branch; RA, rachis; SB, secondary branch. Bar, 100 µm. (f) Phenotype of wild-type cv 9522 and *Osaux1-1;4* mutant inflorescences, showing shorter branches and less spikelets in the mutant. Bar, 5 cm. (g) Panicle length, and the numbers of primary and secondary branches per panicle, in the wild-type cv 9522 and *Osaux1-1;4* mutant inflorescences. Dots represent actual values, and black lines represent mean ± SD, $n = 10$. Asterisks indicate significant differences, ** $P < 0.01$ (Student's *t*-test).

OsER1–OsMKKK10–OsMKK4–OsMPK6 pathway that modulates CK homeostasis to regulate seed size and number (Liu *et al.*, 2015; Guo *et al.*, 2020). Even though *OsMAPK6* was expressed in all 16 inflorescence clusters (Fig. 7a), its spatial–temporal distribution pattern changed across meristem and floret subclusters (Fig. 7b). Consistent with scRNA-seq results, fluorescence from an *OsMAPK6_{pro}-eGFP* marker line could be detected in all inflorescence tissues (Fig. 7c), with highly dynamic signals observed in the IM, BM, and SM (Fig. 7c), supporting its role in meristem activity (Guo *et al.*, 2020). Furthermore, GFP signals were also detected in all spikelet organs, with stronger expression in the palea and lodicule primordia (Fig. 7d). In addition, we also built an *OsGASR1_{pro}-eGFP* marker line to monitor GA response during rice inflorescence development (Furukawa *et al.*, 2006), since GA could modulate Arabidopsis inflorescence architecture in a dynamic pattern, showing a higher GA content in early inflorescence but lower content during flower initiation (Yamaguchi *et al.*, 2014; Kinoshita *et al.*, 2020). Comparable to that of scRNA-seq results (Fig. 7e), highly dynamic GA signals were also observed during early rice reproductive development with lower expression in ePBM and SBM while higher expression in SM (Fig. 7f). Moreover, higher *OsGASR1_{pro}-eGFP* signals were observed in rudimentary glume and SIC while lower expression was detected in outer floral organs, including sterile lemma, lemma, palea, and lodicule (Fig. 7g). Thus, these results provided cellular evidence that phytohormone gradients regulate inflorescence patterning, and the scRNA-seq data provided a comprehensive, reliable cellular atlas of gene expression involved in early rice inflorescence development.

Discussion

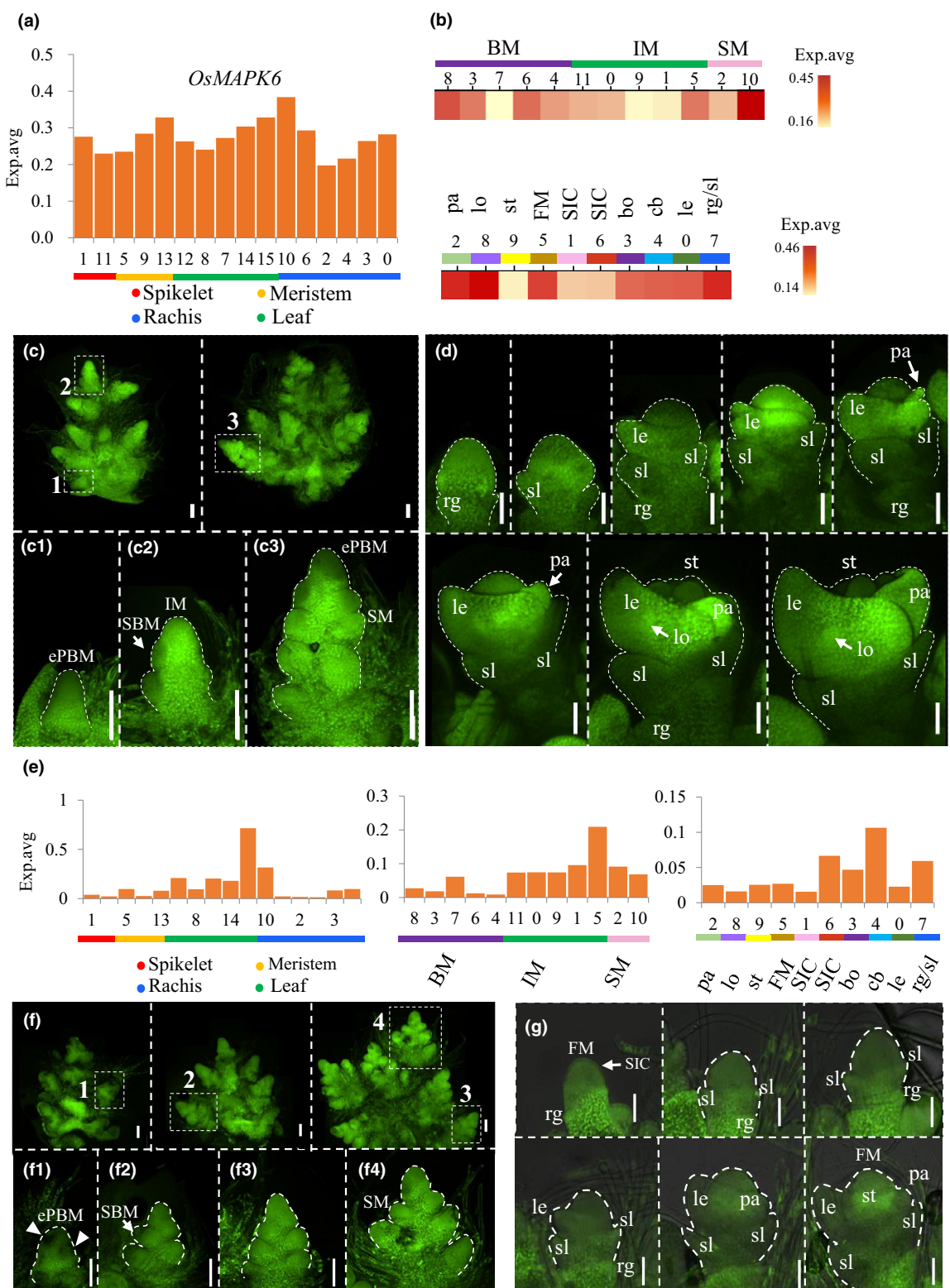
Inflorescence architectures are highly diverse, and their structures have been strongly selected during plant adaptation and crop domestication (Tanaka *et al.*, 2013; Kyozuka, 2014; Kyozuka *et al.*, 2014; Zhang & Yuan, 2014; B. Wang *et al.*, 2018; Yuan *et al.*, 2020; Zhu & Wagner, 2020) [Correction added after first publication 24 February 2022: a reference has been deleted from the preceding sentence]. Great effort has been devoted to unravelling the regulatory processes underlying inflorescence complexity and plasticity and to exploit them for molecular breeding. Here, we reconstructed a transcriptomic atlas covering early rice inflorescence development at the single-cell resolution using scRNA-seq. Although we could not definitively exclude possible side-effects of protoplasting on our scRNA transcriptome, the removal of 61 rice orthologues of 332 protoplast-related genes collected from maize

inflorescence (Table S2) (Xu *et al.*, 2021) did not affect the original clustering, nor the spikelet, floret, and meristem subclustering. This result was consistent with previous reports from maize and Arabidopsis (Ma *et al.*, 2020; Xu *et al.*, 2021; Zhang *et al.*, 2021a) and suggested that protoplasting did not strongly affect our results. However, identification of protoplasting-responsive genes in rice inflorescence samples will further exclude the risk of batch effects caused by protoplasting.

In this work, we captured a series of intermediate cell states during early inflorescence and spikelet development and assigned their highly heterogeneous identities based on well-known marker genes from the literature and results from bioinformatics correlation analyses. Floret subclusters, in particular, could be assigned to discrete reproductive and nonreproductive organs (Fig. 3). We successfully reconstructed the rice floret developmental trajectory over pseudotime ordering, providing cellular evidence that a ‘true’ rice floret comprises the palea, lodicule, and reproductive organs (Fig. 4c,d). Even though there has been no reported canonical *WUSCHEL*-related pathway in rice flower development, we revealed a *DWT1*-mediated WOX pathway that controls FM activity in rice (Figs 3g, S4b,c).

Cells classified as ‘suppressed bract’ and ‘cryptic bract’, whose function has been hypothesized to compete with the meristem or to provide positional signals for meristem determinacy (Chandler, 2012; Whipple, 2017), were identified in meristem and floret subclusters, respectively, each with overlapping (121 conserved genes including *OsSPL14* and *OsSPL17*) but discrete patterns of gene expression (Tables S4, S5). Here, we propose that these cells might have retained meristem activity during domestication, but their identity was repressed by bract-specific genes such as *OsSPL14* and *OsSPL17* (Table S4). Further investigation of the reasons for their retention through intensive selection and breeding may reveal new compensatory mechanisms of meristem activity maintenance.

Though the meristem differentiation trajectory could not be fully reconstructed, the unbiased scRNA-seq in this study revealed that meristems in the inflorescence contain a highly heterogeneous mixture of cell types. Three groups of meristems (IM, BM, and SM) were assigned from 12 meristem subclusters (Fig. 5a), and the reported marker genes were observed to have distinct spatial patterns of expression across the 12 subclusters, exemplified by *SQUAMOSA PROMOTER BINDING PROTEIN*, *WOX*, *YABBY*, *OSH*, and *ROC* family genes (Figs 5b, S6). Some putative regulatory networks that control meristem and floret cell differentiation could be deduced. *LONG PANICLE 1* is one of the IM-enriched genes (Fig. 5b) and was



previously mapped as one of the major candidate quantitative trait loci (QTLs) in controlling panicle length (Liu *et al.*, 2016). Therefore, by integrating data from population genetic studies such as QTLs and genome-wide association studies, the meristem

database here would provide valuable sources to dissect important regulators in meristem differentiation that contribute to breeding. To further assign the functions and identities of these meristem subclusters, *in vivo* marker lines can be developed by

Fig. 7 Expression pattern of *OsMAPK6* and *OsGASR1* genes in inflorescence. (a) *OsMAPK6* expression in inflorescence cell clusters. The y-axis represents the averaged expression value (Exp.avg). (b) Heatmap showing *OsMAPK6* expression pattern in meristem (upper) and floret (lower) cell subclusters. Colours represent the averaged expression value (Exp.avg). BM, branch meristems including the primary branch meristem, elongated primary branch meristem, and secondary branch meristem; SM, spikelet meristem; IM, inflorescence meristem; pa, palea; lo, lodicule; st, stamen; FM, flower meristem; SIC, spikelet identity cell; bo, boundary; cb, cryptic bract; le, lemma; rg, rudimentary glume; sl, sterile lemma. (c) Fluorescence signals in inflorescences of *OsMAPK6_{pro}-eGFP* marker lines, showing dynamic expression in (c₁) BM, (c₂) IM, and (c₃) SM. SBM, secondary branch meristem; ePBM, elongated primary branch meristem. Other abbreviations as in (b). Bar, 100 µm. (d) Fluorescence signals in spikelets of *OsMAPK6_{pro}-eGFP* marker lines, showing increased expression in palea and lodicule. Abbreviations as in (b). Bar, 50 µm. (e) *OsGASR1* expression in (from left to right) inflorescence cell clusters, meristem subclusters, and floret subclusters. The y-axis represents the averaged expression value (Exp.avg). Abbreviations as in (b). (f) Fluorescence signals in inflorescences of *OsGASR1_{pro}-eGFP* marker lines, showing dynamic expression in (f₁) BM, (f₂) IM, and (f₃, f₄) SM. Abbreviations as in (b) and (c). Bar, 100 µm. (g) Fluorescence signals in spikelets of *OsGASR1_{pro}-eGFP* marker lines, showing increased expression in SIC and rg. Abbreviations as in (b). Bar, 50 µm.

selecting cluster-enriched genes revealed by our analyses. A similar strategy could be applied to further examine the developmental trajectory of rachis and leaf cells.

Nevertheless, we provided new genetic evidence for the role of auxin in rice inflorescence development (Fig. 6), and proposed that the *ROC1/HDG* gene family might provide positional signals from the outer layer of the FM to activate rice spikelet and floret initiation (Figs 4f, S4e), which was consistent with findings from Arabidopsis, where the epidermis was proposed as the source of positional signals for meristem maintenance (Gruel *et al.*, 2016). Further comparative study on these meristem genes in rice, and homologous genes in other cereals, might open new windows for understanding how AM differentiation contributes to inflorescence traits. Ultimately, development of a plant regulatory module algorithm for scRNA-seq data, like that in human work (Aibar *et al.*, 2017), and combining it with advanced CRISPR-Cas9 technology, would make step-change improvements in our ability to fully unravel the developmental trajectory of the inflorescence.

Acknowledgements

We thank the Core Facility and Technical Service Center, School of Life Sciences and Biotechnology, Shanghai Jiao Tong University, for assistance with confocal microscopy, Ms Mingjiao Chen and Mr Zhijing Luo for rice planting, and Dr Natalie Betts for editing. This work was supported by the National Natural Science Foundation of China (32170322 and 31671260 to ZY), the Agriculture Research System of Shanghai, China (202103 to ZY), the Open Research Fund of the State Key Laboratory of Hybrid Rice (2018KF07, Hunan Hybrid Rice Research Center), the China–Germany Mobility Program (M-0141), the China Innovative Research Team, Ministry of Education, the Programme of Introducing Talents of Discipline to Universities (111 Project, B14016 to DZ and ZY), and the SMC Morningstar Young Scholarship of Shanghai Jiao Tong University to ZY.

Author contributions

ZY conceived the project. JZ and LW conducted the scRNA-seq experiments. JZ, LB and BZ performed bioinformatics analyses. LW, LZ, XZ and JF collected samples and performed paraffin sectioning, *in situ* hybridization, and phenotyping analyses. LW, LZ and GH constructed CRISPR and marker line vectors. XC performed rice transformation. LC maintained

transgenic plants. DZ, WL and all other authors contributed to the data analysis. JZ, GC and ZY wrote the article, which has been approved by all authors. JZ, LW and LZ contributed equally to this work.

ORCID

- Liming Cao  <https://orcid.org/0000-0001-5315-9224>
Xiaofei Chen  <https://orcid.org/0000-0002-3237-319X>
George Coupland  <https://orcid.org/0000-0001-6988-4172>
Junyi Fan  <https://orcid.org/0000-0001-9702-1147>
Guoqiang Huang  <https://orcid.org/0000-0002-6103-5704>
Wanqi Liang  <https://orcid.org/0000-0002-9938-5793>
Li Wang  <https://orcid.org/0000-0003-4716-4857>
Zheng Yuan  <https://orcid.org/0000-0003-1254-0410>
Dabing Zhang  <https://orcid.org/0000-0003-3181-9812>
Xuelian Zhang  <https://orcid.org/0000-0002-0003-2147>
Lu Zhu  <https://orcid.org/0000-0001-8797-2811>
Jie Zong  <https://orcid.org/0000-0001-6107-3228>

Data availability

All data needed to evaluate the conclusions in the paper are present in the paper and/or the Supporting Information. The GEO accession number for the raw and analysed scRNA-seq data is GSE185068. Additional data related to this paper may be requested from the authors.

References

- Aibar S, González-Blas CB, Moerman T, Huynh-Thu VA, Imrichova H, Hulselmans G, Rambow F, Marine JC, Geurts P, Aerts J *et al.* 2017. SCENIC: single-cell regulatory network inference and clustering. *Nature Methods* 14: 1083–1086.
Becht E, McInnes L, Healy J, Dutertre CA, Kwok IWH, Ng LG, Ginhoux F, Newell EW. 2018. Dimensionality reduction for visualizing single-cell data using UMAP. *Nature Biotechnology* 37: 38–44.
Chandler JW. 2012. Floral meristem initiation and emergence in plants. *Cellular and Molecular Life Sciences* 69: 3807–3818.
Chandler JW, Werr W. 2017. DORNROSCHEN, DORNROSCHEN-LIKE, and PUCHI redundantly control floral meristem identity and organ initiation in Arabidopsis. *Journal of Experimental Botany* 68: 3457–3472.
Chen S, Zhou Y, Chen Y, Gu J. 2018. FASTP: an ultra-fast all-in-one FASTQ preprocessor. *Bioinformatics* 34: i884–i890.
Crow M, Paul A, Ballouz S, Huang ZJ, Gillis J. 2018. Characterizing the replicability of cell types defined by single cell RNA-sequencing data using METANEIGHBOR. *Nature Communications* 9: 884.
Denyer T, Ma X, Klesen S, Scacchi E, Nieselt K, Timmermans MCP. 2019. Spatiotemporal developmental trajectories in the *Arabidopsis* root revealed

- using high-throughput single-cell RNA sequencing. *Developmental Cell* 48: 840–852.e5.
- Dobin A, Davis CA, Schlesinger F, Drenkow J, Zaleski C, Jha S, Batut P, Chaisson M, Gingeras TR. 2013. STAR: ultrafast universal RNA-seq aligner. *Bioinformatics* 29: 15–21.
- Furukawa T, Sakaguchi N, Shimada H. 2006. Two *OsGASR* genes, rice GAST homologue genes that are abundant in proliferating tissues, show different expression patterns in developing panicles. *Genes & Genetic Systems* 81: 171–180.
- Furutani I, Sukegawa S, Kyozuka J. 2006. Genome-wide analysis of spatial and temporal gene expression in rice panicle development. *The Plant Journal* 46: 503–511.
- Gao X, Liang W, Yin C, Ji S, Wang H, Su X, Guo C, Kong H, Xue H, Zhang D. 2010. The *SEPALLATA*-like gene *OsMADS34* is required for rice inflorescence and spikelet development. *Plant Physiology* 153: 728–740.
- Giri J, Bhosale R, Huang G, Pandey BK, Parker H, Zappala S, Yang J, Dievart A, Bureau C, Ljung K et al. 2018. Rice auxin influx carrier *OsAUX1* facilitates root hair elongation in response to low external phosphate. *Nature Communications* 9: e1408.
- Gruel J, Landrein B, Tarr P, Schuster C, Refahi Y, Sampathkumar A, Hamant O, Meyerowitz EM, Jönsson H. 2016. An epidermis-driven mechanism positions and scales stem cell niches in plants. *Science Advances* 2: e1500989.
- Guo T, Lu ZQ, Shan JX, Ye WW, Dong NQ, Lin HX. 2020. *ERECTA1* acts upstream of the OsMKKK10–OsMKK4–OsMPK6 cascade to control spikelet number by regulating cytokinin metabolism in rice. *Plant Cell* 32: 2763–2779.
- Harrop TW, Ud Din I, Gregis V, Osnato M, Jouannic S, Adam H, Kater MM. 2016. Gene expression profiling of reproductive meristem types in early rice inflorescences by laser microdissection. *The Plant Journal* 86: 75–88.
- Hiei Y, Komari T. 2008. Agrobacterium-mediated transformation of rice using immature embryos or calli induced from mature seed. *Nature Protocols* 3: 824–834.
- Higo A, Sahara N, Miura F, Higashi Y, Yamada M, Tamaki S, Ito T, Tarutani Y, Sakamoto T, Fujiwara M et al. 2020. DNA methylation is reconfigured at the onset of reproduction in rice shoot apical meristem. *Nature Communications* 11: e4079.
- Hirano K, Yoshida H, Aya K, Kawamura M, Hayashi M, Hobo T, Sato-Izawa K, Kitano H, Ueguchi-Tanaka M, Matsuoka M. 2017. SMALL ORGAN SIZE 1 and SMALL ORGAN SIZE 2/DWARF AND LOW-TILLERING form a complex to integrate auxin and brassinosteroid signaling in rice. *Molecular Plant* 10: 590–604.
- Hirose N, Makita N, Kojima M, Kamada-Nobusada T, Sakakibara H. 2007. Overexpression of a type-A response regulator alters rice morphology and cytokinin metabolism. *Plant and Cell Physiology* 48: 523–539.
- Horstman A, Fukuoka H, Muino JM, Nitsch L, Guo C, Passarinho P, Sanchez-Perez G, Immink R, Angenent G, Boutilier K. 2015. AIL and HDG proteins act antagonistically to control cell proliferation. *Development* 142: 454–464.
- Hu Y, Liang W, Yin C, Yang X, Ping B, Li A, Jia R, Chen M, Luo Z, Cai Q et al. 2015. Interactions of *OsMADS1* with floral homeotic genes in rice flower development. *Molecular Plant* 8: 1366–1384.
- Ikeda K, Sunohara H, Nagato Y. 2004. Developmental course of inflorescence and spikelet in rice. *Breeding Science* 54: 147–156.
- Ito M, Sentoku N, Nishimura A, Hong SK, Sato Y, Matsuoka M. 2003. Roles of rice GL2-type homeobox genes in epidermis differentiation. *Breeding Science* 53: 245–253.
- Javelle M, Klein-Cosson C, Vernoud V, Boltz V, Maher C, Timmermans M, Depèze-Fargeix N, Rogowsky PM. 2011. Genome-wide characterization of the HD-ZIP IV transcription factor family in maize: preferential expression in the epidermis. *Plant Physiology* 157: 790–803.
- Jean-Baptiste K, McFaline-Figueroa JL, Alexandre CM, Dorrrity MW, Saunders L, Bubb KL, Trapnell C, Fields S, Queitsch C, Cuperus JT. 2019. Dynamics of gene expression in single root cells of *Arabidopsis thaliana*. *Plant Cell* 31: 993–1011.
- Jiao Y, Wang Y, Xue D, Wang J, Yan M, Liu G, Dong G, Zeng D, Lu Z, Zhu X et al. 2010. Regulation of *OsSPL14* by OsmiR156 defines ideal plant architecture in rice. *Nature Genetics* 42: 541–544.
- Karim MR, Hirota A, Kwiatkowska D, Tasaka M, Aida M. 2009. A role for *Arabidopsis PUCHI* in floral meristem identity and bract suppression. *Plant Cell* 21: 1360–1372.
- Kinoshita A, Vayssières A, Richter R, Sang Q, Roggen A, van Driel AD, Smith RS, Coupland G. 2020. Regulation of shoot meristem shape by photoperiodic signaling and phytohormones during floral induction of *Arabidopsis*. *eLife* 9: e60661.
- Kobayashi K, Maekawa M, Miyao A, Hirochika H, Kyozuka J. 2010. *PANICLE PHYTOMER2 (PAP2)*, encoding a SEPALLATA subfamily MADS-box protein, positively controls spikelet meristem identity in rice. *Plant and Cell Physiology* 51: 47–57.
- Kuijt SJ, Greco R, Agalou A, Shao J, 't Hoen CC, Overnas E, Osnato M, Curiale S, Meynard D, van Gulik R et al. 2014. Interaction between the GROWTH-REGULATING FACTOR and KNOTTED1-LIKE HOMEOBOX families of transcription factors. *Plant Physiology* 164: 1952–1966.
- Kyozuka J. 2014. Grass inflorescence. In: Fornara F, ed. *The molecular genetics of floral transition and flower development*. Cambridge, MA, USA: Academic Press, 191–219.
- Kyozuka J, Tokunaga H, Yoshida A. 2014. Control of grass inflorescence form by the fine-tuning of meristem phase change. *Current Opinion in Plant Biology* 17: 110–115.
- Li C, Wang L, Cui Y, He L, Qi Y, Zhang J, Lin J, Liao H, Lin Q, Yang T et al. 2016. Two *FERONIA-like receptor (FLR)* genes are required to maintain architecture, fertility, and seed yield in rice. *Molecular Breeding* 36: e151.
- Li YY, Shen A, Xiong W, Sun QL, Luo Q, Song T, Li ZL, Luan WJ. 2016. Overexpression of *OsHox32* results in pleiotropic effects on plant type architecture and leaf development in rice. *Rice* 9: e46.
- Lin Q, Wang D, Dong H, Gu S, Cheng Z, Gong J, Qin R, Jiang L, Li G, Wang JL et al. 2012. Rice APC/C^{TE} controls tillering by mediating the degradation of MONOCULM 1. *Nature Communications* 3: e752.
- Liu E, Liu Y, Wu G, Zeng S, Tran Thi TG, Liang L, Liang Y, Dong Z, She D, Wang H et al. 2016. Identification of a candidate gene for panicle length in rice (*Oryza sativa* L.) via association and linkage analysis. *Frontiers in Plant Science* 7: e596.
- Liu Q, Liang Z, Feng D, Jiang S, Wang Y, Du Z, Li R, Hu G, Zhang P, Ma Y et al. 2021. Transcriptional landscape of rice roots at the single-cell resolution. *Molecular Plant* 14: 384–394.
- Liu S, Hua L, Dong S, Chen H, Zhu X, Jiang J, Zhang F, Li Y, Fang X, Chen F. 2015. OsMAPK6, a mitogen-activated protein kinase, influences rice grain size and biomass production. *The Plant Journal* 84: 672–681.
- Lu G, Casaretto JA, Ying S, Mahmood K, Liu F, Bi YM, Rothstein SJ. 2017. Overexpression of *OsGATA12* regulates chlorophyll content, delays plant senescence and improves rice yield under high density planting. *Plant Molecular Biology* 94: 215–227.
- Ma X, Denyer T, Timmermans MCP. 2020. PscB: a browser to explore plant single cell RNA-sequencing data sets. *Plant Physiology* 183: 464–467.
- van der Maaten L, Hinton G. 2008. Visualizing data using t-SNE. *Journal of Machine Learning Research* 9: 2579–2605.
- Marand AP, Chen Z, Gallavotti A, Schmitz RJ. 2021. A *cis*-regulatory atlas in maize at single-cell resolution. *Cell* 184: 3041–3055.e21.
- Miura K, Ikeda M, Matsubara A, Song XJ, Ito M, Asano K, Matsuoka M, Kitano H, Ashikari M. 2010. *OsSPL14* promotes panicle branching and higher grain productivity in rice. *Nature Genetics* 42: 545–549.
- Nelms B, Walbot V. 2019. Defining the developmental program leading to meiosis in maize. *Science* 364: 52–56.
- Nishimura A, Ito M, Kamiya N, Sato Y, Matsuoka M. 2002. *OsPNH1* regulates leaf development and maintenance of the shoot apical meristem in rice. *The Plant Journal* 30: 189–201.
- Qiu X, Mao Q, Tang Y, Wang L, Chawla R, Pliner HA, Trapnell C. 2017. Reversed graph embedding resolves complex single-cell trajectories. *Nature Methods* 14: 979–982.
- Ren D, Li Y, Zhao F, Sang X, Shi J, Wang N, Guo S, Ling Y, Zhang C, Yang Z et al. 2013. *MULTI-FLORET SPIKELET1*, which encodes an AP2/ERF protein, determines spikelet meristem fate and sterile lemma identity in rice. *Plant Physiology* 162: 872–884.
- Sakai H, Lee SS, Tanaka T, Numa H, Kim J, Kawahara Y, Wakimoto H, Yang CC, Iwamoto M, Abe T et al. 2013. Rice Annotation Project Database (RAP-DB): an integrative and interactive database for rice genomics. *Plant and Cell Physiology* 54: e6.

- Satija R, Farrell JA, Gennert D, Schier AF, Regev A. 2015. Spatial reconstruction of single-cell gene expression data. *Nature Biotechnology* 33: 495–502.
- Satterlee JW, Strable J, Scanlon MJ. 2020. Plant stem-cell organization and differentiation at single-cell resolution. *Proceedings of the National Academy of Sciences, USA* 117: 33689–33699.
- Schippers JH, Foyer CH, van Dongen JT. 2016. Redox regulation in shoot growth, SAM maintenance and flowering. *Current Opinion in Plant Biology* 29: 121–128.
- Seyfferth C, Renema J, Wendrich JR, Eekhout T, Seurinck R, Vandamme N, Blob B, Saey S, Helariutta Y, Birnbaum KD et al. 2021. Advances and opportunities in single-cell transcriptomics for plant research. *Annual Review of Plant Biology* 72: 847–866.
- Shaw R, Tian X, Xu J. 2021. Single-cell transcriptome analysis in plants: advances and challenges. *Molecular Plant* 14: 115–126.
- Shum EY, Walczak EM, Chang C, Christina Fan H. 2019. Quantitation of mRNA transcripts and proteins using the BD Rhapsody™ single-cell analysis system. In: Suzuki Y, ed. *Single molecule and single cell sequencing*. Singapore City, Singapore: Springer, 63–79.
- Smith T, Heger A, Sudbery I. 2017. UMI_TOOLS: modeling sequencing errors in unique molecular identifiers to improve quantification accuracy. *Genome Research* 27: 491–499.
- Sun H, Qian Q, Wu K, Luo J, Wang S, Zhang C, Ma Y, Liu Q, Huang X, Yuan Q et al. 2014. Heterotrimeric G proteins regulate nitrogen-use efficiency in rice. *Nature Genetics* 46: 652–656.
- Sun S, Wang L, Mao H, Shao L, Li X, Xiao J, Ouyang Y, Zhang Q. 2018. A G-protein pathway determines grain size in rice. *Nature Communications* 9: e851.
- Studi M, Cha JY, Jung MH, Ermawati N, Han CD, Kim MG, Woo YM, Son D. 2012. Potential role of the rice *OsCCS52A* gene in endoreduplication. *Planta* 235: 387–397.
- Suzuki T, Ohneda M, Toriba T, Yoshida A, Hirano HY. 2009. *FON2 SPARE1* redundantly regulates floral meristem maintenance with *FLORAL ORGAN NUMBER2* in rice. *PLoS Genetics* 5: e1000693.
- Tanaka W, Pautler M, Jackson D, Hirano HY. 2013. Grass meristems II: inflorescence architecture, flower development and meristem fate. *Plant and Cell Physiology* 54: 313–324.
- Tanaka W, Toriba T, Hirano HY. 2017. Three *TOB1*-related *YABBY* genes are required to maintain proper function of the spikelet and branch meristems in rice. *New Phytologist* 215: 825–839.
- Tanaka W, Toriba T, Ohmori Y, Yoshida A, Kawai A, Mayama-Tsuchida T, Ichikawa H, Mitsuda N, Ohme-Takagi M, Hirano HY. 2012. The *YABBY* gene *TONGARI-BOUSHI1* is involved in lateral organ development and maintenance of meristem organization in the rice spikelet. *Plant Cell* 24: 80–95.
- Tsuda K, Ito Y, Sato Y, Kurata N. 2011. Positive autoregulation of a *KNOX* gene is essential for shoot apical meristem maintenance in rice. *Plant Cell* 23: 4368–4381.
- Wang B, Smith SM, Li J. 2018. Genetic regulation of shoot architecture. *Annual Review of Plant Biology* 69: 437–468.
- Wang L, Ming L, Liao K, Xia C, Sun S, Chang Y, Wang H, Fu D, Xu C, Wang Z et al. 2021. Bract suppression regulated by the miR156/529-SPLs-NL1-PLA1 module is required for the transition from vegetative to reproductive branching in rice. *Molecular Plant* 14: 1168–1184.
- Wang L, Yin H, Qian Q, Yang J, Huang C, Hu X, Luo D. 2009. *NECK LEAF 1*, a GATA type transcription factor, modulates organogenesis by regulating the expression of multiple regulatory genes during reproductive development in rice. *Cell Research* 19: 598–611.
- Wang L, Zheng K, Zeng L, Xu D, Zhu T, Yin Y, Zhan H, Wu Y, Yang DL. 2022. Reinforcement of CHH methylation through RNA-directed DNA methylation ensures sexual reproduction in rice. *Plant Physiology* 188: 1189–1209.
- Wang QL, Sun AZ, Chen ST, Chen LS, Guo FQ. 2018. SPL6 represses signalling outputs of ER stress in control of panicle cell death in rice. *Nature Plants* 4: 280–288.
- Wang S, Li S, Liu Q, Wu K, Zhang J, Wang S, Wang Y, Chen X, Zhang Y, Gao C et al. 2015a. The *OsSPL16-GW7* regulatory module determines grain shape and simultaneously improves rice yield and grain quality. *Nature Genetics* 47: 949–954.
- Wang S, Sun Z, Wang H, Liu L, Lu F, Yang J, Zhang M, Zhang S, Guo Z, Bent AF et al. 2015b. Rice OsFLS2-mediated perception of bacterial flagellins is evaded by *Xanthomonas oryzae* pvs. *oryzae* and *oryzicola*. *Molecular Plant* 8: 1024–1037.
- Wang W, Li G, Zhao J, Chu H, Lin W, Zhang D, Wang Z, Liang W. 2014. DWARF TILLER1, a WUSCHEL-related homeobox transcription factor, is required for tiller growth in rice. *PLoS Genetics* 10: e1004154.
- Wang Y, Huan Q, Li K, Qian W. 2021. Single-cell transcriptome atlas of the leaf and root of rice seedlings. *Journal of Genetics and Genomics* 48: 881–898.
- Whipple CJ. 2017. Grass inflorescence architecture and evolution: the origin of novel signaling centers. *New Phytologist* 216: 367–372.
- Wils CR, Kaufmann K. 2017. Gene-regulatory networks controlling inflorescence and flower development in *Arabidopsis thaliana*. *Biochimica et Biophysica Acta (BBA) – Gene Regulatory Mechanisms* 1860: 95–105.
- Wu D, Liang W, Zhu W, Chen M, Ferrández C, Burton RA, Dreni L, Zhang D. 2018. Loss of LOFSEP transcription factor function converts spikelet to leaf-like structures in rice. *Plant Physiology* 176: 1646–1664.
- Wu Q, Xu F, Liu L, Char SN, Ding Y, Je BI, Schmelz E, Yang B, Jackson D. 2020. The maize heterotrimeric G protein beta subunit controls shoot meristem development and immune responses. *Proceedings of the National Academy of Sciences, USA* 117: 1799–1805.
- Xie K, Minkenberg B, Yang Y. 2015. Boosting CRISPR/Cas9 multiplex editing capability with the endogenous rRNA-processing system. *Proceedings of the National Academy of Sciences, USA* 112: 3570–3575.
- Xu C, Wang Y, Yu Y, Duan J, Liao Z, Xiong G, Meng X, Liu G, Qian Q, Li J. 2012. Degradation of MONOCULM 1 by APC/C^{TAD1} regulates rice tillering. *Nature Communications* 3: e750.
- Xu C, Crow M, Rice BR, Li F, Harris B, Liu L, Demesa-Arevalo E, Lu Z, Wang L, Fox N et al. 2021. Single-cell RNA sequencing of developing maize ears facilitates functional analysis and trait candidate gene discovery. *Developmental Cell* 56: 557–568 e556.
- Yaari G, Bolen CR, Thakar J, Kleinstein SH. 2013. Quantitative set analysis for gene expression: a method to quantify gene set differential expression including gene–gene correlations. *Nucleic Acids Research* 41: e170.
- Yamaguchi N, Winter CM, Wu MF, Kanno Y, Yamaguchi A, Seo M, Wagner D. 2014. Gibberellin acts positively then negatively to control onset of flower formation in *Arabidopsis*. *Science* 344: 638–641.
- Yang S, Yu Q, Zhang Y, Jia Y, Wan S, Kong X, Ding Z. 2018. ROS: the fine-tuner of plant stem cell fate. *Trends in Plant Science* 23: 850–853.
- Yoshikawa T, Ito M, Sumikura T, Nakayama A, Nishimura T, Kitano H, Yamaguchi I, Koshiba T, Hibara K, Nagato Y et al. 2014. The rice *FISH BONE* gene encodes a tryptophan aminotransferase, which affects pleiotropic auxin-related processes. *The Plant Journal* 78: 927–936.
- Yu C, Sun C, Shen C, Wang S, Liu F, Liu Y, Chen Y, Li C, Qian Q, Aryal B et al. 2015. The auxin transporter, OsAUX1, is involved in primary root and root hair elongation and in Cd stress responses in rice (*Oryza sativa* L.). *The Plant Journal* 83: 818–830.
- Yu G, Wang LG, Han Y, He QY. 2012. CLUSTERPROFILER: an R package for comparing biological themes among gene clusters. *OMICS: A Journal of Integrative Biology* 16: 284–287.
- Yuan H, Qin P, Hu L, Zhan S, Wang S, Gao P, Li J, Jin M, Xu Z, Gao Q et al. 2019. OsSPL18 controls grain weight and grain number in rice. *Journal of Genetics and Genomics* 46: 41–51.
- Yuan Z, Persson S, Zhang D. 2020. Molecular and genetic pathways for optimizing spikelet development and grain yield. *aBIOTECH* 1: 276–292.
- Zhang D, Yuan Z. 2014. Molecular control of grass inflorescence development. *Annual Review of Plant Biology* 65: 553–578.
- Zhang TQ, Chen Y, Liu Y, Lin WH, Wang JW. 2021a. Single-cell transcriptome atlas and chromatin accessibility landscape reveal differentiation trajectories in the rice root. *Nature Communications* 12: e2053.
- Zhang TQ, Chen Y, Wang JW. 2021b. A single-cell analysis of the *Arabidopsis* vegetative shoot apex. *Developmental Cell* 56: 1056–1074.e8.
- Zhang TQ, Xu ZG, Shang GD, Wang JW. 2019. A single-cell RNA sequencing profiles the developmental landscape of *Arabidopsis* root. *Molecular Plant* 12: 648–660.

- Zheng K, Wang L, Zeng L, Xu D, Guo Z, Gao X, Yang DL. 2021. The effect of RNA polymerase V on 24-nt siRNA accumulation depends on DNA methylation contexts and histone modifications in rice. *Proceedings of the National Academy of Sciences, USA* 118: e2100709118.
- Zhu Y, Wagner D. 2020. Plant inflorescence architecture: the formation, activity, and fate of axillary meristems. *Cold Spring Harbor Perspectives in Biology* 12: a034652.
- Zou LP, Sun XH, Zhang ZG, Liu P, Wu JX, Tian CJ, Qiu JL, Lu TG. 2011. Leaf rolling controlled by the homeodomain leucine zipper class IV gene *Roc5* in rice. *Plant Physiology* 156: 1589–1602.

Supporting Information

Additional Supporting Information may be found online in the Supporting Information section at the end of the article.

Fig. S1 Data quality and single-cell landscape for rice inflorescence.

Fig. S2 Inflorescence cell type identification.

Fig. S3 Marker genes in floret cells.

Fig. S4 Cell type identification in all floret cells, and floret phenotypes of wild-type and *dwt1* lines and *in situ* hybridization analysis of *ROC* genes.

Fig. S5 Overview of single-cell landscape for inflorescence meristem.

Fig. S6 Expression of meristem marker genes.

Fig. S7 Differentiation trajectory of meristem cells.

Fig. S8 Information about *Osaux1* mutations.

Table S1 Primers used in this study.

Table S2 Protoplasting-related genes collected from maize.

Table S3 Raw data and clean data quality statistics.

Table S4 Enriched and reported marker genes.

Table S5 Gene Ontology analysis of all cell type and differentially expressed genes.

Table S6 Differentially expressed genes and branched expression analysis modelling.

Table S7 Quantitative set analysis for gene expression related pathways.

Please note: Wiley Blackwell are not responsible for the content or functionality of any Supporting Information supplied by the authors. Any queries (other than missing material) should be directed to the *New Phytologist* Central Office.